# Intraseasonal descriptors and extremes in South African rainfall. Part I: summer climatology and statistical characteristics.

Asmat Ullah, Benjamin Pohl, Julien Pergaud, Bastien Dieppois, Mathieu Rouault

# Intraseasonal Descriptors and Extremes in South African rainfall. Part I: Summer Climatology and Statistical Characteristics

**Ullah, A., Pohl, B., Pergaud, J., Dieppois, B. & Rouault, M.**



**Original citation & hyperlink:**
Ullah, A, Pohl, B, Pergaud, J, Dieppois, B & Rouault, M 2022, 'Intraseasonal Descriptors and Extremes in South African rainfall. Part I: Summer Climatology and Statistical Characteristics', *International Journal of Climatology*, vol. 42, no. 9, pp. 4538-4563.
https://dx.doi.org/10.1002/joc.7489

DOI 10.1002/joc.7489
ISSN 0899-8418
ESSN 1097-0088

Publisher: Wiley

# Intraseasonal Descriptors and Extremes in South African rainfall. Part I: Summer Climatology and Statistical Characteristics

Asmat Ullah[1]* ; Benjamin Pohl[1] ; Julien Pergaud[1] ; Bastien Dieppois[2] ; Mathieu Rouault[3]

[1] Biogéosciences, UMR6282 CNRS / Université de Bourgogne Franche-Comté, Dijon, France

[2] Centre for Agroecology, Water and Resilience, Coventry University, Coventry, UK

[3] Nansen Tutu Center for Marine Environmental Research, Department of Oceanography, University of Cape Town, South Africa



**International Journal of Climatology**

**Revised: 30 November 2021**

*** Corresponding Author's Address**

Asmat Ullah: asmat-786@hotmail.com

Laboratoire Biogéosciences
Université de Bourgogne
6 Boulevard Gabriel
21000 DIJON − FRANCE

## Abstract

Rainfall extremes are of major and increasing importance in semi-arid countries and their variability has strong implications for water resource and climate impacts on the local societies and environment. Here, we examine intraseasonal descriptors (ISDs) and wet extremes in austral summer rainfall (November−February) over South Africa (SA). Using daily observations from 225 rain gauges and ERA5 reanalysis between 1979 and 2015, we propose a novel typology of wet extreme events based on their spatial fraction, thus differentiating large- and small-scale extremes. Long-term variability of both types of extreme rainfall events is then extensively discussed in the context of ISDs.

The results demonstrate that using 7% of spatial fraction simultaneously exceeding the local threshold of the 90$^{th}$ percentile produces remarkable results in characterizing rainfall extremes into large- and small-scale extremes. Austral summer total rainfall is found to be primarily shaped by large-scale extremes which constitute more than half of the rainfall amount under observation, and nearly half in ERA5. Observation (ERA5) shows an average of 8±5 (20±7) days per season associated with large-scale extremes, which are comprised in 5±3 (10±3) spells with an average persistence of at least 2 days. Overall, we find a strong dependence of total rainfall on the number of wet days and wet spells that are associated with large-scale extremes. We also find that large- and small-scale extremes are well-organized and spatially coherent in nature yet extreme conditions during small-scale events are found sporadic over the region, contrasting with large-scale events for which extreme conditions are found over a larger and coherent region.





## Key-Words

South Africa — Intraseasonal Descriptors — Rainfall Extremes — Climate Variability — Spatial coherence

## 1. Introduction

Most of South Africa (SA hereafter) experiences a rainy season in austral summer (November to February; Pohl *et al.*, 2014; Favre *et al.*, 2016). Located at the interface between the tropics and the mid-latitudes of the Southern Hemisphere, while being surrounded by two thermally contrasted oceans (Rouault *et al.*, 2003), SA is subject to both the influence of tropical convection and temperate dynamics (Washington and Todd, 1999; Hart *et al.*, 2010; Vigaud *et al.*, 2012). Together with highly heterogeneous vegetation and topography, these tropical and temperate influences form a mosaic of climates in association with contrasted surface atmospheric characteristics such as rainfall amount and temperature which strongly vary in time and space. Like many semi-arid regions in the tropics, SA depends heavily on the quality of its rainy seasons, as irrigation remains rather rare in this region (Crétat *et al.*, 2012; Masupha *et al.*, 2016). Thus, rainfall variability and forecasting at fine spatial and temporal scales are a matter of crucial importance for SA agriculture and economy (Conway *et al.*, 2015).

In SA, during the austral summer, precipitation events are generally associated with moist atmospheric convection, ranging in scale from single-cell storms to organized systems, such as Mesoscale Convective Complexes (MCCs; Blamey and Reason, 2013), squall lines (Rouault *et al.*, 2002) and tropical storms (Reason and Keibel, 2004; Reason, 2007; Malherbe *et al.*, 2012, 2014; Fitchett and Grab, 2014). Cut-off lows (COLs) can also lead to extreme rainfall in SA, but they are rare during the summer season (Favre *et al.*, 2013). In austral summer, three key regions (namely southwest Indian Ocean, tropical western Indian Ocean, and tropical southeast Atlantic Ocean) are known to inject moisture flux into the southern African continent (Desbiolles *et al.*, 2018; Rapolaki *et al.*, 2019, 2020). The dominant rain-bearing systems over the region are synoptic-scale cloud bands, known locally as Tropical Temperate Troughs (TTTs; Manhique *et al.*, 2011; Hart *et al.*, 2013; Macron *et al.*, 2014; James *et al.*, 2020). TTTs correspond to synoptic-scale cloud bands that link tropical instability over the subcontinent with an upper-tropospheric frontal system embedded in the mid-latitude westerly circulation (Todd and Washington, 1999; Todd *et al.*, 2004; Hart *et al.*, 2010) and bring about 30–60% of summer rainfall over subtropical SA (Hart *et al.*, 2013; Macron *et al.*, 2014). The remaining 40–70% of the summer rainfall amounts are provided by rain-bearing mechanisms linked to tropical

convection, such as regional thermal low-pressure (Reason *et al.*, 2006) or the Madden-Julian Oscillation (MJO; Pohl *et al.*, 2007). Rapolaki *et al.* (2019) highlighted that, over the Limpopo River Basin, 48% of extreme events are associated with TTTs, 28% with tropical low-pressure systems, 14% with mesoscale convective systems, and 10% with COLs.

Intraseasonal descriptors (hereafter ISDs) are defined as wet and dry sequences of days during the rainy season (Ratan and Venugopal, 2013; Gitau *et al.*, 2015, 2018). Examining ISDs provides various intrinsic characteristics of a rainy season, such as the average number of wet and dry days, persistence of spells, intensity of wet spells and total rainfall. Similar studies focused on other regions, such as equatorial East Africa (Camberlin *et al.*, 2009; Moron *et al.*, 2013; Gitau *et al.*, 2015, 2018; Philippon *et al.*, 2015), have already demonstrated their relevance and usefulness in climate diagnostics and prediction. However, analyses devoted to ISDs remain quite rare in SA. Tennant and Hewitson (2002) found that anomalously wet rainy seasons tend to experience a larger number of heavy rainy days (>20 $mm.day^{-1}$). Cook *et al.* (2004) highlighted that moisture anomalies between wet and dry spells were strongly related to the Kalahari low. They also stated that wet years were characterized by longer and more intense wet spells, rather than by a greater number of wet spells (Cook *et al.*, 2004). Similarly, previous studies found a strong relationship between dry spells and El Niño Southern Oscillation (ENSO), suggesting potential predictability of ISDs using this relationship (Usman and Reason, 2004; Reason *et al.*, 2005; Crétat et al. 2012.). Physically, El Niño conditions could act to shift TTTs eastwards over the Mozambique Channel (Nicholson and Kim, 1997; Cook, 2000, 2001; Misra, 2003; Nicholson, 2003; Dieppois *et al.*, 2015, 2016, 2019), thereby enhancing the number of dry spells over the continent. The relationship between TTTs and ENSO has been confirmed and further documented by Fauchereau *et al.* (2009) and Pohl *et al.* (2018). During La Niña a low-pressure develop over southern Africa, which is related to anomalous upward motion and enhanced moisture fluxes into and over the region which results in rainfall surplus while El Niño is linked with high-pressure over southern Africa, which is associated with anomalous downward motion and reduced moisture fluxes into and over the region which result in rainfall deficit during austral summer season (Ratnam *et al.*, 2014; Hoell *et al.*, 2015).

The severity and frequency of wet and dry extreme events are likely to increase at the global scale as a response to anthropogenic emissions of greenhouse gases (Donat *et al.*, 2016). This statement is also true for SA rainfall (Mason and Joubert, 1997; Mason *et al.*, 1999; Shongwe *et al.*, 2009; Engelbrecht *et al.*, 2013; Pinto *et al.*, 2016). Future scenarios include a combination of decreasing numbers of rainy days and increasing intensity of extreme rainy days (Pohl *et al.*, 2017), which are likely to modify the intrinsic characteristics of intraseasonal spells in the future.

This study aims to provide fundamental and up-to-date knowledge about the intrinsic characteristics of wet and dry ISDs. First, we provide an overall assessment of ISDs, in which extremes are embedded using the latest available observation archive and a state-of-the-art reanalysis product. This study then proposes a novel typology of extreme rainfall events, based on their spatial fraction as a base criterion, disentangling rainfall events into large-scale and small-scale extremes. To our knowledge, there is hitherto no study that addresses the spatial dimension in the definition of rainfall extremes over the region, despite its importance for predictions over other regions (Lu *et al.*, 2017; Oueslati *et al.*, 2017). In this paper, we calculate and discuss the intrinsic characteristics of large- and small-scale extremes in the context of ISDs over SA. The contribution made should be of interest for a wide range of the scientific community working on seasonal forecasts. Such results also have considerable importance for stakeholders in the environmental, agricultural, energy, water and economic sectors. A companion paper will further assess how these different types of extreme events vary in time, and/or are modulated by modes of large-scale variability at different timescales ranging from the synoptic scale to decadal variability.

This paper (Part I), more specifically dedicated to the mean characteristics of rainfall extremes in SA, is organized as follows. Section 2 presents datasets and methodology. Section 3 provides an assessment of wet and dry ISDs and their summer climatology over SA. Section 4 is dedicated to defining criteria to identify extreme rainfall events and to facilitate their categorization into large- and small-scale extreme events. Section 5 addresses an assessment of large- and small-scale rainfall extremes in the definition of ISDs. Section 6 summarizes the results and establishes the main conclusions.

## 2. Data and Methodology

### 2.1. In-situ and reanalysis data

Observed daily rainfall data from 225 stations (hereafter OBS), spanning 50 years between 1965 and 2015, in which missing values represent less than 1%, were retrieved from the archives of the Water Research Commission of South Africa, which constitutes a dense network of 2625 stations (http://www.wrc.org.za; Fig. 1a).

In addition, we used state-of-the-art ERA5 reanalysis to compare and cross-validate our results. ERA5 reanalysis (Copernicus Climate Change Service, 2017; Hersbach *et al.*, 2020) is the 5th generation reanalysis available from the European Center for Medium-Range Weather Forecasts (ECMWF), providing 0.25° × 0.25° resolution of hourly gridded outputs of surface and atmospheric fields at the global scale, spanning 1979 to the present. ERA5 has now been extended to 1950–1978 but the lack of assimilation of satellite data before 1979 raises the question of the homogeneity of the dataset, the detailed evaluation of which is mandatory before using it. However, it is not the scope of the present study, hence our choice to consider a common period of 36-years (1979–2015).

To focus on the summer rainfall regions, a seasonality test was then applied on OBS and ERA5 (Crétat *et al.*, 2012). Using the seasonality test, only the stations and grid-points for which at least 50% of annual rainfall occurred during an extended austral summer (October to March) were retained. The spatial distribution of the percentage of summer rainfall in OBS and ERA5 is presented in Figure 1a-b. Regarding ERA5, all grid-points (AGP) and those nearest to OBS (NN) were used in this study. The Comparing the NN and AGP fields of ERA5 is particularly important in order to examine whether the network is dense enough to study rainfall extremes. The NN and AGP fields of ERA5 have here been named ERA5−NN and ERA5−AGP, respectively.

To define new metrics accounting for the typology of rainfall extremes, we focused on the austral summer season (October−March), and we analyzed two distinct baseline periods (1965−2015) for OBS and (1979−2015) for ERA5. By considering extended austral summer seasons and the two distinct baseline periods for the computation of 90$^{th}$ percentile values, we gained two advantages: i) a longer period for OBS ensures statistical robustness of low-

frequency decadal variability; ii) longer seasons also include rainfall onset (October) and cessation (March) months (discussed later in the companion paper). For all remaining objectives, we restricted the study to the period dating 1979−2015 and to the core of the rainy season (November−February).

## 2.2. Methods

### 2.2.1. Definition of intraseasonal descriptors at the regional scale

A threshold of 1.0 mm.day$^{-1}$ was used to delineate wet from dry days (Gitau *et al.*, 2013, 2015). A unified definition for wet and dry spells was obtained as suggested in several previous studies (Ratan and Venugopal, 2013; Gitau *et al.*, 2015, 2018). A wet (dry) spell is defined as a duration of *"i"* wet (dry) days preceded and followed by a dry (wet) day. As summarized in Table 1a-b, various ISDs, which are associated with wet and dry spells, are computed for each station and grid-point using OBS and ERA5. Multi-year variability of each ISD is then assessed using seasonal average computed at the regional scale (cf. Section 3).

To quantify and compare temporal variability, commonly used statistical metrics were applied to each ISD: mean (μ), standard deviation (SD), root mean square error (RMSE) and coefficient of variation (CV: Asmat and Athar, 2017; Asmat *et al.*, 2018). The Mann Kendall (MK) non-parametric test was used to perform the trend analysis (Mann, 1945; Kendall, 1957). Pearson's correlations were computed to quantify the dependence of total rainfall on ISDs.

### 2.2.2. Assessment of rainfall extremes

***a) Local threshold for rainfall extremes***

We first computed the 90$^{th}$ percentile of daily rainfall amount of each station and grid-point, which were retrieved from the aforementioned seasonality test, over the two climatological baseline periods as described in Section 2.1. The 90$^{th}$ percentile values were calculated by removing all values below 1.0 mm.day$^{-1}$ for more robust identification of extreme rainfall events. The comparisons of the spatial distributions of the 90$^{th}$ percentile, as calculated before and after removing non-rainy and drizzle days (i.e. days with less than 1.0 mm), are presented in Figure 2a-b and Figure 2c-d respectively. This choice made the evaluation less sensitive to measurement accuracy and to the tendency of some numerical models to produce an excessive number of drizzle events (Frei *et al.*, 2003; Gitau *et al.*, 2015; Maraun, 2016). A similar sensitivity to

drizzle days was found to be more pronounced in ERA5; thus, not removing drizzle days would have led to underestimating the 90$^{th}$ percentiles. The 90$^{th}$ percentile threshold is calculated based on a normal distribution, and we note that it did not significantly differ from one calculated based on a theoretical extreme value distribution (Gumbel distribution, cf. Fig S1c-d). This suggests the statistical robustness of the approach used to calculate the extreme thresholds in this study.

***b) Regional threshold for rainfall extremes***

A novel typology of rainfall extremes based on the spatial fraction of rainfall events is then proposed. The spatial fraction of an extreme event is defined as the number of stations or grid-points that simultaneously reach the 90$^{th}$ percentile regardless of their location on the day of the event. A similar methodology has been successfully used for the identification of heat waves in West Africa (Oueslati *et al.*, 2017). The principal reason for using the spatial fraction as a base criterion is to differentiate localized, or small-scale extreme events from large-scale extreme events. On one hand, small-scale extreme events are related to isolated convective cells and therefore stochastic in nature, rendering them highly unpredictable. On the other hand, large-scale extreme events are embedded in large-scale modes of climate variability, hence potentially more predictable. The spatial fraction of extreme events depends on the density of the network, but also on its anisotropy, which is likely to cause some issues in the estimation of the spatial extension of the events because the stations are not uniformly distributed in space. In reference to this assumption, the spatial fraction of events is here quantified using both the ERA5−NN and ERA5−AGP fields. The comparison between ERA5−NN and ERA5−AGP fields makes it possible to assess whether or not the network is dense enough to study rainfall extremes. The density might not be sufficient if ERA5−NN exhibits substantially different properties than in ERA5−AGP. Thus, a caution is required to interpret the results related to large- and small-scale extremes as: i) the extremes are not characterized here based on environmental consequences but from an atmospheric point of view considering the characteristics of rainfall field itself; ii) considering the use of administrative boundaries, limitation in observation along with using NN and AGP fields of ERA5 yet there is a likelihood that some events that may have major environmental consequences, are not necessarily captured; iii) resolution of reanalysis is

particularly important to capture small-scale extreme events. Section 4.1 addresses a brief assessment conducted in defining a robust and relevant threshold of spatial fraction.

### *c) Spatial characteristics of rainfall extremes*

Based on the defined threshold of spatial fraction, we first separated all days associated with large- and small-scale extreme events (cf. Section 4.1). The average characteristics of both types of extremes were then assessed in terms of frequency and intensity for each station and grid point. The frequency and intensity were computed based on two criteria: i) average number of days exceeding the 1.0 mm threshold during large- and small-scale extreme events; ii) average number of days exceeding the 90$^{th}$ percentile threshold during large- and small-scale extreme events. For the sake of clarity, in this paper, this analysis is only provided for OBS (cf. Section 4.2).

### *d) Spatial coherence of rainfall extremes*

An analysis addressing the spatial coherence of large- and small-scale extremes is also provided. Here, we analyze the density of stations recording rainfall on the days of large- and small-scale extremes based on the same method used to address the spatial characteristics of extreme events i.e.: i) considering all stations recording rainfall >1.0 mm on the day of the event; ii) considering only those stations which exceeded their 90$^{th}$ percentile on the day of the event. The density of the stations was assessed using a narrow bin size of 0.5°, corresponding to the stations that are located within approximately 55 kilometers over latitudes and 43 kilometers over longitudes (cf. Section 4.3).

## 2.2.3. Definition of intraseasonal descriptors associated with rainfall extremes

Large- and small-scale extreme rainy days were first obtained from the typology of rainfall extremes (cf. Section 4). Both types of events were then explicitly considered in the context of ISDs. By placing these events in the framework of ISDs, we were able to further explore the climatology and intrinsic properties of such events on an interannual timescale. Thus, several ISDs associated with large- and small-scale rainfall extremes were assessed using OBS and ERA5. A brief description of extreme ISDs is presented in Table 2. To quantify and compare

temporal variability and trends, the same statistical metrics as introduced in Section 2.2.1 are used in Section 5.

# 3. ISDs at the regional scale

## 3.1. Multi-year variability of ISDs

The average spatial distribution of each ISD is presented in Figure 3. A spatial gradient from southwest to northeast clearly prevails in all ISDs, as northeastern regions are much wetter than southern regions in all wet ISDs (Fig. 3a). Meanwhile, dry ISDs show larger values over the southwestern regions denoting drier conditions (Fig. 3b), in agreement with Crétat *et al.* (2012). When compared with OBS, ERA5 displays nearly realistic responses for all ISDs in terms of spatial distribution but shows some biases when spatial average is assessed (cf. Figure S2). Notably, ERA5 overestimates the values in all wet ISDs, except for the intensity of wet spells (Fig. S2a). Such overestimations of seasonal rainfall in ERA5 could be related to a higher number of wet spells with weaker intensity (WS and WSI panels in Fig. 3 and 4). In addition, looking at the spatial distribution of biases in ISDs, we note that the intensity of wet spells is underestimated throughout the region (WSI panel in Fig. S3b). Meanwhile, the overestimation of the number of wet days is more pronounced from the northeast to the southwest (WD panel in Fig. S3b). ERA5 also largely underestimates the number of wet spells, especially in regions of higher altitude (>1400 m above sea level), such as the Drakensberg region (WS panel in Fig. S3b). This suggests that ERA5 struggles to break the continuity of rainy days within a spell, which results in fewer but more prolonged spells (WS and WSP panels in Fig. S3b).

Reanalysis bias over the African continent across three generations of ECMWF reanalysis is extensively discussed in Gleixner *et al.* (2020). This study highlights substantial improvements in ERA5 achieved by improved model physics and data assimilation schemes. In this study, we still note significant discrepancies between ERA5 and observations in ISDs as discussed above. The foremost problem in ERA5 is its ability to produce a realistic response for those regions characterized by a complex terrain (Wang *et al.*, 2019), given the fact that such regions tend to have a lower number of observations. In SA, the average biases that we find in intraseasonal characteristics could also result from similar constraints, since the northeastern part of SA is characterized by a complex topography that often enhances the biases present in numerical models (Favre *et al.*, 2016; Koseki *et al.*, 2018).

Figure 4 presents the statistical distribution and multi-year variability of ISDs. Both ERA5−NN and ERA5−AGP fields show consistent results in all wet and dry ISDs (see violin plots in Fig. 4), suggesting that the density of observational archives used for OBS (i.e. 225 stations) is sufficient to monitor the spatial and temporal variability of ISDs throughout SA. Regarding wet ISDs, OBS and ERA5 display an average of 20±4 and 44±6 days over a season, respectively (WD panel in Fig. 4a). These wet days are driven by 13±2 spells for OBS and 17±2 spells for ERA5 (WS panel in Fig. 4a). For OBS (ERA5), the austral summer season is composed of 90 (70) dry days and 12 (16) dry spells (DD and DS panels in Fig. 4b). Although biases exist in ERA5, multi-year variability appears realistic with a statistically significant correlation (>0.8) to OBS for most of the wet and dry ISDs (Table 3).

The average number of wet days exceeding the 90$^{th}$ percentiles is 2 and 4 in OBS and ERA5, respectively ($WD_{P90}$ panel in Fig. 4a). As discussed above, ERA5 also overestimates the number of wet days, including the number of wet days exceeding the 90$^{th}$ percentiles. The temporal patterns of extreme wet days and total rainfall show coherent peaks in both ISDs between 1993−94 and 1999−2000 ($WD_{P90}$ and TR panels in Fig. 4a), which clearly indicates that the wettest years tend to correspond to the largest seasonal occurrences of extremes. Overall, the CV remains higher OBS in most of wet and dry ISDs as compared to ERA5, whereas ERA5−NN exhibits slightly lower RMSE as compared to ERA5−AGP (Table 3). No significant trends appear in any ISD, except in the intensity of wet spells, which increases in OBS (ERA5−AGP) at a rate of +3.23 (+2.06) mm.day$^{-1}$, based on the Mann Kendall trend test at p=0.05 (Table 3).

### 3.2. Contribution of ISDs to total seasonal rainfall

The relationship between total rainfall and ISDs was assessed using point-wise correlation (Fig. 5). Overall, all wet ISDs exhibit a positive correlation with total rainfall, but the wet spells show a negative correlation over the northeastern regions in ERA5 (WS panels in Fig. 5a). Such negative correlations between wet spells and total rainfall over the northeastern regions, where the elevation is the highest, may once again highlight the limitation of ERA5 over complex terrains (cf. Figure S3). Regarding the relationship between dry ISDs (Thoithi *et al.*, 2020) and total rainfall, a significant negative relationship logically prevails (Fig. 5b).

The correlation of two ISDs, WD and $WD_{P90,}$ with total rainfall is particularly strong, exceeding 0.8 (significant at p=0.05) in almost all grid-points (WD and $WD_{P90}$ panels in Fig. 5a). This indicates that the anomalously wet seasons primarily correspond to a higher number of wet and extreme wet days, thereby confirming the results of Tennant and Hewitson (2002). In addition to point-wise correlations, we also estimated the contributions of ISDs to austral summer rainfall at the regional scale, using spatially averaged time series (lower right corner of each panel in Fig. 5). The highest correlations are >0.94 and significant at p=0.05 and are found for WD and $WD_{P90,}$ consistently with the point-wise correlations. This highlights the critical importance of the two ISDs in shaping the rainfall variability over SA.

# 4. Rainfall extremes

## 4.1. Typology of extreme rainfall events

Here, we use the average spatial fraction of extreme rainfall events as a base criterion to differentiate large- and small-scale extreme events. Theoretically, large-scale extreme events should be embedded in large-scale modes of climate variability, and therefore show greater potential predictability. Meanwhile, small-scale extreme events are more likely related to isolated or organized convective cells, such as MCCs, which are stochastic in nature, and thus less predictable (Blamey and Reason, 2013). Thus, large-scale extreme events must exhibit a higher fraction of stations or grid-points simultaneously reaching the extreme threshold as compared to small-scale extremes. Moreover, it is also reasonable to speculate that large-scale extreme events are less frequent as compared to small-scale extremes in the austral summer season. To differentiate the characteristics of these two contrasting types of extremes, we assess here their multivariate distributions in terms of duration, spatial fraction, frequency and intensity (Fig. 6).

Defining a robust and relevant threshold for the spatial fraction of events was critically important. Given the aforementioned biases in the reanalysis, we rely solely on OBS to develop a relevant definition for the typology of extreme rainfall events (upper two panels in Fig. 6). In OBS, the higher event intensity (>27 $mm.day^{-1}$) and lower frequency lies above a spatial fraction of 7% (Fig. 6). A threshold of 7% for the spatial fraction therefore appears to be a good compromise to differentiate large- and small-scale extreme events. In order to assess the sensitivity to this threshold, we also considered 5% and 6% thresholds, and quantified the

differences in the average characteristics of small- and large-scale extremes by assessing them in the context of ISDs. We found that, using other thresholds, large-scale extremes resulted in high frequency, thus obscuring distinct characteristics as compared to small-scale extremes (results not shown). The physical properties and the variability of the extreme rainfall events retrieved from the typology are further discussed in the context of ISDs in Section 5.

### 4.2. Spatial characteristics of rainfall extremes

Figure 7a (left panel) displays the average frequency of days exceeding the 1.0 mm threshold during large-scale extreme events for each station. Stations located along the preferable location of continental TTTs (bringing rainfall over SA: Fauchereau *et al.*, 2009; Macron *et al.*, 2014) tend to exhibit the highest frequency, which accounts for 4−7 days.season$^{-1}$ (left panel in Fig. 7a). This suggests that synoptic scale rain-bearing systems could be responsible for large-scale extremes. When considering the 90$^{th}$ percentile threshold, an average frequency of 1−4 days.season$^{-1}$ was shown by all stations during large-scale extreme events (right panel in Fig. 7a). It is interesting to note that each station exhibits extreme conditions from 1 to 4 times in a season. However, for each event, in order to qualify as a large-scale extreme event, at least 7% of the stations should attain their 90$^{th}$ percentile threshold on the same day. This suggests that during each event, a distinct set of stations responds with extreme conditions which depend exclusively on the synoptic features of the rain-bearing system and storm track. When analyzing the intensity of large-scale extreme events by considering either the 1.0 mm or 90$^{th}$ percentile threshold, we note that the intensity of large-scale events is spatially uniform. This finding thus suggests that such extreme events bring sustained extreme conditions over the entire region (Fig. 7c).

Different patterns of event frequency emerge when examining small-scale extremes (Fig. 7b). Here, a SW−NE gradient prevails, especially when event frequency is computed by considering the 90$^{th}$ percentile threshold (right panel in Fig 7b). In particular, northeastern parts of SA show a higher frequency of small-scale extremes. These results are consistent with the findings of Blamey and Reason (2013) who demonstrated that the northeastern region of SA is the preferable location of MCCs. A SW−NE gradient is also quite visible for event intensity when computed by considering the 1.0 mm threshold (left panel in Fig. 7d). No remarkable differences

appear over the region when the intensity is computed by considering the 90$^{th}$ percentile threshold (right panel in Fig. 7d). This result may be explained by the fact that the 90$^{th}$ percentile threshold of each station remains the same for large- and small-scale extremes.

In summary, a uniform distribution of frequency and intensity, computed either by considering the 1.0 mm or the 90$^{th}$ percentile threshold, indicates that large-scale extremes result from coherent rain-bearing systems with uniform extreme conditions throughout the spatial extension of the events. Meanwhile, during small-scale extreme events the extreme conditions largely prevail over the northeastern parts of SA.

### 4.3. Spatial coherence of rainfall extremes

In this section, we assess the spatial coherence of large- and small-scale extremes. This analysis is particularly important in the context of large-scale extremes as it indicates whether extreme conditions during events are: i) uniformly distributed over the spatial extension of the events, suggesting that large-scale extremes are spatially coherent; ii) sporadically located, suggesting there could be an aggregation of small-scale events occurring at the same time.

Figure 8 presents the density of the stations exceeding 1.0 mm.day$^{-1}$ during the large-scale extreme events according to their latitude and longitude. A well-organized, nearly unimodal distribution of station density clearly prevails during all large-scale extreme events, fitting well with the distribution of the stations in the observational network. This suggests that the latter are spatially coherent in nature. Figure 9 duplicates this analysis for the core of the large-scale extreme events, where rainfall intensity causes the extreme threshold excess (i.e. only the stations exceeding their local 90$^{th}$ percentile of daily rainfall amounts). These stations also display organized and spatially coherent patterns, with unimodal distributions clearly prevailing. This suggests that during these events, the extreme wet conditions also show strong spatial coherence, most events being characterized by one single large-scale core rather than many smaller ones. Taken together, the results displayed in Figures 8-9 lead us to discard the hypothesis of several smaller and/or scattered events occurring at the same time. They also increase our confidence in the method used here to track large-scale rainfall extremes in SA.

The same analysis was then replicated for small-scale extreme events. As small-scale events are higher in number, for the sake of clarity we show the results for the month of January only (similar results were obtained for the other months and are not shown). Figure S4 shows the collective response of stations recording >1.0 mm.day$^{-1}$ of rainfall during small-scale extreme events. Small-scale extreme events also exhibit an organized extension of rain-bearing systems over latitudes and longitudes, but with slightly fewer stations in each bin (Fig. S4). Figure S5 displays the number of stations exceeded their 90$^{th}$ percentile in each 0.5° bin during the small-scale extreme events. Interestingly, we notice that extreme conditions occur only sporadically and locally over the region during small-scale events (Fig. S5). Over longitudes, the over-representation of events located between 28°E and 33°E could denote the influence of MCCs over eastern SA (Fig. S5b), confirming the results reported by Blamey and Reason (2013). Taken together, these results suggest that the spatial extension of the rain-bearing system remains quite similar between small-scale and large-scale events, suggesting that they have the same physical nature (except for a larger proportion of MCCs in the case of small-scale extremes). However, the core regions associated with heavy rainfall dramatically change, showing that the rain-bearing systems mostly differ in the size of their core, bringing the largest rainfall amounts and thereby causing the climatic wet extreme.

In summary, analyzing the spatial coherence of rainfall extremes provides a remarkable advantage in monitoring the collective behavior of all stations during extreme events. The results demonstrate that using a 7% threshold of spatial extension as a base criterion to differentiate large- and small-scale extremes is robust and leads to separate events that drastically differ in terms of spatial coherence. Although both types of extremes can be considered as spatially coherent, as rainfall events occur over a large region at the same time, extreme conditions only occur sporadically over the region during small-scale events, contrasting with large-scale events for which extreme conditions are found over a larger and coherent region. This suggests that the nature of corresponding rain-bearing systems is the same, but that their intensity changes, an issue that will be further discussed and explored in Part II.

## 5. Intraseasonal characteristics of rainfall extremes

In this section, large- and small-scale extreme rainfall events are examined in the context of ISDs.

### 5.1. Multi-year variability of large-scale rainfall extremes

The average characteristics and multi-year variability of ISDs associated with large-scale extremes are displayed in Figure 10a. OBS (ERA5) shows an average of 8±5 (20±7) days associated with large-scale extremes, which are included in 5±3 (10±3) spells.season$^{-1}$, with an average persistence of 2 days ($WD_{EXT,}$ $WS_{EXT}$ and $WSP_{EXT}$ panels in Fig. 10a). In OBS (ERA5) total rainfall of about 167±36 (129±30) mm.season$^{-1}$ is driven by wet spells associated with large-scale extreme events ($TR_{EXT}$ panels in Fig. 10a). The multi-year variability of ISDs is well captured by ERA5−NN and ERA5−AGP fields, with statistically significant correlations to OBS at $p<0.05$ (Table 4a). Nevertheless, the intensity of wet spells remains highly underestimated by ERA5−NN and ERA5−AGP which shows average wet spell intensity of about 25.49 and 25.21 mm.day$^{-1}$ respectively ($WSI_{EXT}$ panels in Fig. 10a). In addition, in OBS, larger seasonal rainfall variability seems related to the smaller number of wet spells and wet days, as well as more intense events, but this is not identified in ERA5. Importantly, the observational network is found to be dense enough to study the variability of extreme ISDs associated with large-scale rainfall extremes, since there are no major differences in the results obtained with ERA5−NN and −AGP (Fig. 10a). In all ISDs associated with large-scale extreme events, the CV remains higher in OBS than in ERA5 (Fig. 10a). Meanwhile, ERA5−NN exhibits lower RMSE as compared to ERA5−AGP, when computed with respect to OBS (Table 4). No significant trend appears in most ISDs, except a significant increase of 2.30 spells.season$^{-1}$ identified in the observed number of wet spells, based on the Mann Kendall trend test at $p=0.05$ (Table 4a).

Relationships between seasonal total rainfall and ISDs associated with large-scale extremes are presented in Figure 11a. In all datasets, large-scale extreme ISDs exhibit strong positive correlations with total rainfall (significant at $p<0.05$), except for the intensity of wet spells (Fig. 11a). Overall, we find a strong association between seasonal total rainfall and the number of wet days and wet spells associated with large-scale extremes, as identified in OBS. The performance of ERA5 is still weaker, especially in the relationship between wet spells and total rainfall. This

leads to conclusions similar to those presented in Section 3 above, regarding the limitations of ERA5 in producing realistic wet spells and intensity.

## 5.2. Multi-year variability of small-scale rainfall extremes

Analysis of ISDs associated with small-scale extremes is presented in Figure 10b. In OBS (ERA5), the frequency of days associated with small-scale extremes is 80±9 (48±7 for NN and 64±7 for AGP), with an average frequency of 19±3 (24±3) spells.season$^{-1}$ ($WD_{EXT}$ and $WS_{EXT}$ panels in Fig. 10b). These spells are, by construction, highly localized in space, with an average spatial extension of 1.5%−2.5% over the SA domain, but they do exhibit a persistence of 2−4 days on average ($WSP_{EXT}$ and $ME_{EXT}$ panels in Fig. 10b). OBS and ERA5 fields show average wet spells intensity of about 41.86 and 21.49−22.14 mm.day$^{-1}$ ($WSI_{EXT}$ panels in Fig. 10b) which is quite like the average wet spell intensities noted for large-scale extremes. The plausible explanation of this similar behavior is that both types of extremes are first tracked by using local 90$^{th}$ percentile threshold which is indeed same for each station or grid-point. These extremes are recognized differently in terms of spatial fraction (number of stations or grid-points which exceed the 90$^{th}$ percentile threshold simultaneously during a spell; cf. Section 4.1).

In ERA5 (especially ERA−NN) and OBS, a significant trend appears in the intensity of wet spells associated with small-scale extreme events indicating a +2.0 mm.day$^{-1}$ average increase in the spell's intensity (Table 4). Although the contribution of small-scale extremes to total rainfall is quite low as compared to that of large-scale extremes, the increasing trend in the intensity of such highly localized storms could nonetheless have crucial importance, especially for the agricultural sector, among others. Such intensification of rainfall extremes could be a consequence of ongoing climate change (Kendon *et al.*, 2017, 2019; Pohl *et al.*, 2017) and could be due to the so-called Clausius-Clapeyron scaling, linking air warming trends to rainfall intensity increase through hygrometry (Betts and Harshvardhan, 1987; Trenberth *et al.*, 2003; Pall *et al.*, 2006; Kharin *et al.*, 2007; O'Gorman and Schneider, 2009; Muller *et al.*, 2011; Westra *et al.*, 2014). The relationship between the ISDs associated with small-scale extremes and the seasonal total rainfall amount is presented in Figure 11b. Except for the relationship between wet days associated with small-scale extremes and total rainfall, we note weak or negative relationships between ISDs and total rainfall (Fig. 11b). Table 4 summarizes the relevant statistics for small-scale extreme ISDs.

The role of small-scale extremes in shaping total rainfall variability is moderate in austral summer. One plausible explanation for this is that the small-scale extremes are highly localized and are embedded in spatially coherent rain-bearing systems, which are mostly associated with non-extreme rainfall conditions over the region, as already discussed in Section 4.4. ERA5 fields show contrasting behaviors in small-scale extremes, as opposed to the results reported for large-scale extreme in Section 5.1. In addition, the long-term variability of a few small-scale extreme ISDs (i.e. wet spells and wet spell intensity) is not fully realistic in ERA5, as demonstrated by weaker and non-significant correlations between both ERA5 fields and OBS (Table 4b). On the other hand, weaker yet significant correlations between ERA5 fields and OBS ranging from 0.42−0.79 are noted in other small-scale extreme ISDs (Table 4b). This implies that the density of the observational network might not be sufficient to detect most of these highly localized small-scale events, and/or that higher resolution reanalysis is required to skillfully capture these events.

### 5.3. Respective contribution of large- and small-scale extremes to seasonal rainfall amount

Figure 12 displays the contribution of large-scale, small-scale and non-extreme rainfall to seasonal total rainfall amount. In OBS (ERA5), total rainfall associated with large-scale extremes shows an average contribution of about 58% (41%−45%), against 11% (6%) for small-scale extremes (see, pie plots in Figure 12). This shows how dependent the region is on a small number of events that concentrate most of the rainfall. Although ERA5 overestimates austral summer rainfall amounts (Section 3.1), it underestimates the contribution of rainfall extremes to total amounts. In ERA5, summer rainfall is mainly driven by non-extreme events, as opposed to OBS, where more than half of the summer rains seem to be associated with large-scale extreme events. The biases in ERA5 may result from an overestimation of the spatial extension of rain-bearing systems over the region, due to: i) perfectible model physics and/or strong internal variability, e.g. to simulate the small-scale atmospheric convection, and/or; ii) a limited amount of available radiosonde data to constrain the reanalysis, or an assimilation technique that could extend atmospheric instability over too large regions.

Interestingly, during the 1981−82 and 1991−92 seasons, large-scale extremes do not contribute to rainfall amount, as rainfall is mostly driven by non-extreme rainfall in OBS (contributing to

>90%; Fig. 12). These two seasons are, however, extremely dry, with seasonal rainfall amounts 30%−42% lower than normal, as noted in OBS (Fig. 12). Such results are not found in ERA5, although a closer examination of these two seasons reveals that: i) total rainfall deficit also exist in ERA5 which accounts up to 22%−40%, which is quite close to the OBS (see, TR panel in Fig. 3); ii) ERA5 overestimates total rainfall and spatial fraction, which is why ERA5 could capture the few large-scale extreme events during these seasons (see, $TR_{EXT}$ and $SF_{EXT}$ panels in Fig. 10a). In addition, these two seasons correspond to strong El Niño episodes, and it is well-understood that El Niño episodes can favor dry conditions over SA, and particularly large rainfall deficits (see, for instance, Dieppois *et al.*, 2015, 2016, 2019; Pascale *et al.*, 2019).

On the contrary, in 1996−97 and 2000−01, the contribution of large-scale extremes to total rainfall amount exceeds 79%. Results from these wettest seasons tie in well with previous studies (Hoell and Cheng, 2018), highlighting a synchronous influence of La Niña, active Angola Low and SIOD phasing, bringing together a substantial surplus of rainfall over SA over those specific seasons. It is therefore likely that such connections do exist between rainfall extremes and different modes of variability. Thus, in the companion paper, we attempt to provide a comprehensive assessment of how rainfall extremes respond under low (interannual and decadal) and high (intraseasonal and synoptic) frequency modes of climate variability.

## 6. Conclusions and discussion

This study first examines the average characteristics of wet and dry intraseasonal descriptors in South Africa during the austral summer season from 1979 to 2015. A focus is then placed on extreme daily rainfall events. Using OBS and ERA5 reanalysis, extreme rainfall events are grouped into two types, according to their spatial fraction, separating large-scale and small-scale extremes. An investigation is then carried out to examine the spatial coherence of such extremes. Finally, for the first time in a region-wide study, large- and small-scales of extremes are explicitly assessed in the definition of intraseasonal descriptors.

The observational network of 225 stations provides an adequate spatial resolution to examine general rainfall characteristics and large-scale extremes in terms of intraseasonal descriptors. This is also true for ERA5, as the reanalysis performs remarkably well in the analysis of large-scale extremes, when analyzed using its nearest neighbor and all-grid-point fields. Nevertheless,

compared to OBS, ERA5 shows larger biases in reproducing small-scale extremes, thereby confirming that such reanalysis is primarily suited to analysis of large-scale climate processes and mechanisms.

Strong correlations between wet days (including extreme wet days) and total rainfall indicates that anomalously wet seasons generally correspond to higher numbers of extreme events. Summer SA rainfall is found to be primarily associated with large-scale extremes, which account for more than half of the seasonal amount in OBS, and nearly half of it in ERA5. The contribution and variability of small-scale extremes are not consistent across datasets and remain quite low. Moreover, the density of the observational network and the spatial resolution of current global reanalysis might not be sufficient to skillfully capture these events.

This study is a first step towards a more profound understanding of rainfall extremes in the region. The results demonstrate that using a threshold of 7% network density as base criterion and as a metric for the spatial fraction produces good quality results in characterizing rainfall extremes over the region. The 7% threshold used to differentiate large- vs small scale events is found not only relevant for the observational network, but also for ERA5-NN and ERA5-AGP. Based on our results, we find that large-scale extremes are well-organized and spatially coherent in nature. Meanwhile, small-scale extreme events, which might be related to mesoscale convective complexes, are highly localized in space and prevail largely over the northeastern parts of SA.

An added value of this work resides in the first presentation of a detailed mapping of rainfall variability over South Africa, including large- and small-scale extreme events, as well as non-extreme rainfall contribution. Such studies have immediate and considerable implications for theoretical and applied climate variability-based studies. These include, but are not limited to, societal sectors related to environment and energy, hydrology modeling and water resource management, and more specifically to agriculture, especially given the fact that South Africa is highly dependent on rain-fed agriculture.

In the companion paper (Part II) of this study, we attempt to assess the relationships of large- and small-scale extremes with low-frequency (interannual- and decadal-scale) and high-frequency (intraseasonal- and synoptic-scale) modes of variability. Such a typology of extremes will also be

completed by considering their duration which is particularly important to differentiate short- and long-lived large-scale events. The latter may be considered as potentially high-impact rainfall events leading to high environmental or societal impacts, a question of major and ever-increasing importance under climate change.

**Acknowledgements**

This work is part of the I-SITE Bourgogne Franche-Comté Junior Fellowship IMVULA (AAP2-JF-06). It was also supported by the NRF SARCHI chair on "modeling ocean-atmosphere-land interactions" and the Nansen Tutu Centre for Marine studies. Calculations were performed using HPC resources from DNUM CCUB (Centre de Calcul de l'Université de Bourgogne).

## References


Asmat U, Athar H. 2017. Run-based multi-model interannual variability assessment of precipitation and temperature over Pakistan using two IPCC AR4-based AOGCMs. *Theoretical and Applied Climatology*, 127(1–2). https://doi.org/10.1007/s00704-015-1616-6.

Asmat U, Athar H, Nabeel A, Latif M. 2018. An AOGCM based assessment of interseasonal variability in Pakistan. *Climate Dynamics*. Springer Berlin Heidelberg, 50(1–2): 349–373. https://doi.org/10.1007/s00382-017-3614-0.

Betts AK, Harshvardhan. 1987. Thermodynamic constraint on the cloud liquid water feedback in climate models. *Journal of Geophysical Research: Atmospheres*. John Wiley & Sons, Ltd, 92(D7): 8483–8485. https://doi.org/10.1029/JD092ID07P08483.

Blamey RC, Reason CJC. 2013. The role of mesoscale convective complexes in southern Africa summer rainfall. *Journal of Climate*, 26(5): 1654–1668. https://doi.org/10.1175/JCLI-D-12-00239.1.

Camberlin P, Moron V, Okoola R, Philippon N, Gitau W. 2009. Components of rainy seasons' variability in Equatorial East Africa: Onset, cessation, rainfall frequency and intensity. *Theoretical and Applied Climatology*, 98(3–4): 237–249. https://doi.org/10.1007/s00704-009-0113-1.

Conway D, Van Garderen EA, Deryng D, Dorling S, Krueger T, Landman W, Lankford B, Lebek K, Osborn T, Ringler C, Thurlow J, Zhu T, Dalin C. 2015. Climate and southern Africa's water-energy-food nexus. *Nature Climate Change*. Nature Publishing Group, 5(9): 837–846. https://doi.org/10.1038/nclimate2735.

Cook C, Reason CJC, Hewitson BC. 2004. Wet and dry spells within particularly wet and dry summers in the South African summer rainfall region. *Climate Research*, 26(1): 17–31. https://doi.org/10.3354/cr026017.

Cook KH. 2000. The South Indian convergence zone and interannual rainfall variability over Southern Africa. *Journal of Climate*, 13(21): 3789–3804. https://doi.org/10.1175/1520-0442(2000)013<3789:TSICZA>2.0.CO;2.

Cook KH. 2001. A southern hemisphere wave response to ENSO with implications for Southern Africa precipitation. *Journal of the Atmospheric Sciences*, 58(15): 2146–2162. https://doi.org/10.1175/1520-0469(2001)058<2146:ASHWRT>2.0.CO;2.

Copernicus Climate Change Service (C3S). 2017. ERA5: Fifth generation of ECMWF atmospheric reanalyses of the global climate. *Copernicus Climate Change Service Climate Data Store (CDS), accessed 2018-05-04*.

Crétat J, Richard Y, Pohl B, Rouault M, Reason C, Fauchereau N. 2012. Recurrent daily rainfall patterns over South Africa and associated dynamics during the core of the austral summer. *International Journal of Climatology*, 32(2): 261–273. https://doi.org/10.1002/joc.2266.

Desbiolles F, Blamey R, Illig S, James R, Barimalala R, Renault L, Reason C. 2018. Upscaling impact of wind/sea surface temperature mesoscale interactions on southern Africa austral

summer climate. *International Journal of Climatology*, 38(12): 4651–4660. https://doi.org/10.1002/joc.5726.

Dieppois B, Pohl B, Crétat J, Eden J, Sidibe M, New M, Rouault M, Lawler D. 2019. Southern African summer-rainfall variability, and its teleconnections, on interannual to interdecadal timescales in CMIP5 models. *Climate Dynamics*. Springer Berlin Heidelberg, 53(5–6): 3505–3527. https://doi.org/10.1007/s00382-019-04720-5.

Dieppois B, Pohl B, Rouault M, New M, Lawler D, Keenlyside N. 2016. Interannual to interdecadal variability of winter and summer southern African rainfall, and their teleconnections. *Journal of Geophysical Research*. https://doi.org/10.1002/2015JD024576.

Dieppois B, Rouault M, New M. 2015. The impact of ENSO on Southern African rainfall in CMIP5 ocean atmosphere coupled climate models. *Climate Dynamics*, 45(9–10): 2425–2442. https://doi.org/10.1007/s00382-015-2480-x.

Donat MG, Lowry AL, Alexander L V., O'Gorman PA, Maher N. 2016. More extreme precipitation in the world's dry and wet regions. *Nature Climate Change*. https://doi.org/10.1038/nclimate2941.

Engelbrecht CJ, Engelbrecht FA, Dyson LL. 2013. High-resolution model-projected changes in mid-tropospheric closed-lows and extreme rainfall events over southern Africa. *International Journal of Climatology*, 33(1): 173–187. https://doi.org/10.1002/joc.3420.

Fauchereau N, Pohl B, Reason CJC, Rouault M, Richard Y. 2009. Recurrent daily OLR patterns in the Southern Africa/Southwest Indian ocean region, implications for South African rainfall and teleconnections. *Climate Dynamics*, 32(4): 575–591. https://doi.org/10.1007/s00382-008-0426-2.

Favre A, Hewitson B, Lennard C, Cerezo-Mota R, Tadross M. 2013. Cut-off Lows in the South Africa region and their contribution to precipitation. *Climate Dynamics*, 41(9–10): 2331–2351. https://doi.org/10.1007/s00382-012-1579-6.

Favre A, Philippon N, Pohl B, Kalognomou EA, Lennard C, Hewitson B, Nikulin G, Dosio A, Panitz HJ, Cerezo-Mota R. 2016. Spatial distribution of precipitation annual cycles over South Africa in 10 CORDEX regional climate model present-day simulations. *Climate Dynamics*. Springer Berlin Heidelberg, 46(5–6): 1799–1818. https://doi.org/10.1007/s00382-015-2677-z.

Fitchett JM, Grab SW. 2014. A 66-year tropical cyclone record for south-east Africa: Temporal trends in a global context. *International Journal of Climatology*, 34(13): 3604–3615. https://doi.org/10.1002/joc.3932.

Frei C, Christensen JH, Déqué M, Jacob D, Jones RG, Vidale PL. 2003. Daily precipitation statistics in regional climate models: Evaluation and intercomparison for the European Alps. *Journal of Geophysical Research: Atmospheres*, 108(3): 1–19. https://doi.org/10.1029/2002jd002287.

Gitau W, Camberlin P, Ogallo L, Bosire E. 2018. Trends of intraseasonal descriptors of wet and dry spells over equatorial eastern africa. *International Journal of Climatology*, 38(3): 1189–

1200. https://doi.org/10.1002/joc.5234.

Gitau W, Camberlin P, Ogallo L, Okoola R. 2015. Oceanic and atmospheric linkages with short rainfall season intraseasonal statistics over Equatorial Eastern Africa and their predictive potential. *International Journal of Climatology*, 35(9): 2382–2399. https://doi.org/10.1002/joc.4131.

Gitau W, Ogallo L, Camberlin P, Okoola R. 2013. Spatial coherence and potential predictability assessment of intraseasonal statistics of wet and dry spells over Equatorial Eastern Africa. *International Journal of Climatology*, 33(12): 2690–2705. https://doi.org/10.1002/joc.3620.

Gleixner S, Demissie T, Diro GT. 2020. Did ERA5 improve temperature and precipitation reanalysis over East Africa? *Atmosphere*, 11(9): 1–19. https://doi.org/10.3390/atmos11090996.

Hart NCG, Reason CJC, Fauchereau N. 2010. Tropical-extratropical interactions over southern Africa: Three cases of heavy summer season rainfall. *Monthly Weather Review*, 138(7): 2608–2623. https://doi.org/10.1175/2010MWR3070.1.

Hart NCG, Reason CJC, Fauchereau N. 2013. Cloud bands over southern Africa: Seasonality, contribution to rainfall variability and modulation by the MJO. *Climate Dynamics*, 41(5–6): 1199–1212. https://doi.org/10.1007/s00382-012-1589-4.

Hersbach H, Bell B, Berrisford P, Hirahara S, Horányi A, Muñoz-Sabater J, Nicolas J, Peubey C, Radu R, Schepers D, Simmons A, Soci C, Abdalla S, Abellan X, Balsamo G, Bechtold P, Biavati G, Bidlot J, Bonavita M, De Chiara G, Dahlgren P, Dee D, Diamantakis M, Dragani R, Flemming J, Forbes R, Fuentes M, Geer A, Haimberger L, Healy S, Hogan RJ, Hólm E, Janisková M, Keeley S, Laloyaux P, Lopez P, Lupu C, Radnoti G, de Rosnay P, Rozum I, Vamborg F, Villaume S, Thépaut JN. 2020. The ERA5 global reanalysis. *Quarterly Journal of the Royal Meteorological Society*, 146(730): 1999–2049. https://doi.org/10.1002/qj.3803.

Hoell A, Cheng L. 2018. Austral summer Southern Africa precipitation extremes forced by the El Niño-Southern oscillation and the subtropical Indian Ocean dipole. *Climate Dynamics*. Springer Berlin Heidelberg, 50(9–10): 3219–3236. https://doi.org/10.1007/s00382-017-3801-z.

Hoell A, Funk C, Magadzire T, Zinke J, Husak G. 2015. El Niño–Southern Oscillation diversity and Southern Africa teleconnections during Austral Summer. *Climate Dynamics*. Springer Berlin Heidelberg, 45(5–6): 1583–1599. https://doi.org/10.1007/s00382-014-2414-z.

James R, Hart NCG, Munday C, Reason CJC, Washington R. 2020. Coupled climate model simulation of tropical–extratropical cloud bands over Southern Africa. *Journal of Climate*, 33(19): 8579–8602. https://doi.org/10.1175/JCLI-D-19-0731.1.

Kendall MG. 1957. *Rank Correlation Methods. 4th Edition*. *Charles Griffin, London*.

Kendon EJ, Ban N, Roberts NM, Fowler HJ, Roberts MJ, Chan SC, Evans JP, Fosser G, Wilkinson JM. 2017. Do convection-permitting regional climate models improve projections of future precipitation change? *Bulletin of the American Meteorological Society*, 98(1): 79–93. https://doi.org/10.1175/BAMS-D-15-0004.1.

Kendon EJ, Stratton RA, Tucker S, Marsham JH, Berthou S, Rowell DP, Senior CA. 2019.

Enhanced future changes in wet and dry extremes over Africa at convection-permitting scale. *Nature Communications*. Springer US, 10(1). https://doi.org/10.1038/s41467-019-09776-9.

Kharin V V., Zwiers FW, Zhang X, Hegerl GC. 2007. Changes in Temperature and Precipitation Extremes in the IPCC Ensemble of Global Coupled Model Simulations. *Journal of Climate*. American Meteorological Society, 20(8): 1419–1444. https://doi.org/10.1175/JCLI4066.1.

Koseki S, Pohl B, Bhatt BC, Keenlyside N, Njouodo ASN. 2018. Insights into the summer diurnal cycle over Eastern South Africa. *Monthly Weather Review*, 146(12): 4339–4356. https://doi.org/10.1175/MWR-D-18-0184.1.

Lu E, Zhao W, Zou X, Ye D, Zhao C, Zhang Q. 2017. Temporal-spatial monitoring of an extreme precipitation event: Determining simultaneously the time period it lasts and the geographic region it affects. *Journal of Climate*, 30(16): 6123–6132. https://doi.org/10.1175/JCLI-D-17-0105.1.

Macron C, Pohl B, Richard Y, Bessafi M. 2014. How do tropical temperate troughs form and develop over Southern Africa? *Journal of Climate*, 27(4): 1633–1647. https://doi.org/10.1175/JCLI-D-13-00175.1.

Malherbe J, Engelbrecht FA, Landman WA, Engelbrecht CJ. 2012. Tropical systems from the southwest Indian Ocean making landfall over the Limpopo River Bassouthern Africa: A historical perspective. *International Journal of Climatology*, 32(7): 1018–1032. https://doi.org/10.1002/joc.2320.

Malherbe J, Landman WA, Engelbrecht FA. 2014. The bi-decadal rainfall cycle, Southern Annular Mode and tropical cyclones over the Limpopo River Basin, southern Africa. *Climate Dynamics*, 42(11–12): 3121–3138. https://doi.org/10.1007/s00382-013-2027-y.

Manhique AJ, Reason CJC, Rydberg L, Fauchereau N. 2011. ENSO and Indian Ocean sea surface temperatures and their relationships with tropical temperate troughs over Mozambique and the Southwest Indian Ocean. *International Journal of Climatology*, 31(1): 1–13. https://doi.org/10.1002/joc.2050.

Mann H. 1945. Mann Nonparametric test against trend. *Econometrica*.

Maraun D. 2016. Bias Correcting Climate Change Simulations - a Critical Review. *Current Climate Change Reports*. Current Climate Change Reports, 2(4): 211–220. https://doi.org/10.1007/s40641-016-0050-x.

Mason SJ, Goddard L, Graham NE, Yulaeva E, Sun L, Arkin PA. 1999. The IRI seasonal climate prediction system. *WRPMD 1999: Preparing for the 21st Century*. https://doi.org/10.1061/40430(1999)4.

Mason SJ, Joubert AM. 1997. Simulated changes in extreme rainfall over southern Africa. *International Journal of Climatology*, 17(3): 291–301. https://doi.org/10.1002/(sici)1097-0088(19970315)17:3<291::aid-joc120>3.3.co;2-t.

Masupha TE, Moeletsi ME, Tsubo M. 2016. Dry spells assessment with reference to the maize crop in the Luvuvhu River catchment of South Africa. *Physics and Chemistry of the Earth*.

https://doi.org/10.1016/j.pce.2015.10.014.

Misra V. 2003. The influence of Pacific SST variability on the precipitation over southern Africa. *Journal of Climate*, 16(14): 2408–2418. https://doi.org/10.1175/2785.1.

Moron V, Camberlin P, Robertson AW. 2013. Extracting subseasonal scenarios: An alternative method to analyze seasonal predictability of regional-scale tropical rainfall. *Journal of Climate*, 26(8): 2580–2600. https://doi.org/10.1175/JCLI-D-12-00357.1.

Muller CJ, O'Gorman PA, Back LE. 2011. Intensification of Precipitation Extremes with Warming in a Cloud-Resolving Model. *Journal of Climate*. American Meteorological Society, 24(11): 2784–2800. https://doi.org/10.1175/2011JCLI3876.1.

Nicholson S. 2003. Comments on "The South Indian convergence zone and interannual rainfall variability over southern Africa" and the question of ENSO's influence on southern Africa. *Journal of Climate*, 16(3): 555–562. https://doi.org/10.1175/1520-0442(2003)016<0555:COTSIC>2.0.CO;2.

Nicholson SE, Kim J. 1997. The relationship of the el MNO-southern oscillation to African rainfall. *International Journal of Climatology*, 17(2): 117–135. https://doi.org/10.1002/(SICI)1097-0088(199702)17:2<117::AID-JOC84>3.0.CO;2-O.

O'Gorman PA, Schneider T. 2009. Scaling of Precipitation Extremes over a Wide Range of Climates Simulated with an Idealized GCM. *Journal of Climate*. American Meteorological Society, 22(21): 5676–5685. https://doi.org/10.1175/2009JCLI2701.1.

Oueslati B, Pohl B, Moron V, Rome S, Janicot S. 2017. Characterization of heat waves in the Sahel and associated physical mechanisms. *Journal of Climate*, 30(9): 3095–3115. https://doi.org/10.1175/JCLI-D-16-0432.1.

Pall P, Allen MR, Stone DA. 2006. Testing the Clausius–Clapeyron constraint on changes in extreme precipitation under CO2 warming. *Climate Dynamics 2006 28:4*. Springer, 28(4): 351–363. https://doi.org/10.1007/S00382-006-0180-2.

Pascale S, Pohl B, Kapnick SB, Zhang H. 2019. On the Angola low interannual variability and its role in modulating ENSO effects in southern Africa. *Journal of Climate*, 32(15): 4783–4803. https://doi.org/10.1175/JCLI-D-18-0745.1.

Philippon N, Camberlin P, Moron V, Boyard-Micheau J. 2015. Anomalously wet and dry rainy seasons in Equatorial East Africa and associated differences in intra-seasonal characteristics. *Climate Dynamics*. Springer Berlin Heidelberg, 45(7–8): 2101–2121. https://doi.org/10.1007/s00382-014-2460-6.

Pinto I, Lennard C, Tadross M, Hewitson B, Dosio A, Nikulin G, Panitz HJ, Shongwe ME. 2016. Evaluation and projections of extreme precipitation over southern Africa from two CORDEX models. *Climatic Change*, 135(3–4): 655–668. https://doi.org/10.1007/s10584-015-1573-1.

Pohl B, Dieppois B, Crétat J, Lawler D, Rouault M. 2018. From synoptic to interdecadal variability in southern African rainfall: Toward a unified view across time scales. *Journal of Climate*, 31(15): 5845–5872. https://doi.org/10.1175/JCLI-D-17-0405.1.

Pohl B, MacRon C, Monerie PA. 2017. Fewer rainy days and more extreme rainfall by the end of the century in Southern Africa. *Scientific Reports*. Nature Publishing Group, 7(April): 6–12. https://doi.org/10.1038/srep46466.

Pohl B, Richard Y, Fauchereau N. 2007. Influence of the Madden-Julian oscillation on southern African summer rainfall. *Journal of Climate*, 20(16): 4227–4242. https://doi.org/10.1175/JCLI4231.1.

Pohl B, Rouault M, Roy S Sen. 2014. Simulation of the annual and diurnal cycles of rainfall over South Africa by a regional climate model. *Climate Dynamics*, 43(7–8): 2207–2226. https://doi.org/10.1007/s00382-013-2046-8.

Rapolaki RS, Blamey RC, Hermes JC, Reason CJC. 2019. A classification of synoptic weather patterns linked to extreme rainfall over the Limpopo River Basin in southern Africa. *Climate Dynamics*. Springer Berlin Heidelberg, 53(3–4): 2265–2279. https://doi.org/10.1007/s00382-019-04829-7.

Rapolaki RS, Blamey RC, Hermes JC, Reason CJC. 2020. Moisture sources associated with heavy rainfall over the Limpopo River Basin, southern Africa. *Climate Dynamics*. Springer Berlin Heidelberg, 55(5–6): 1473–1487. https://doi.org/10.1007/s00382-020-05336-w.

Ratan R, Venugopal V. 2013. Wet and dry spell characteristics of global tropical rainfall. *Water Resources Research*, 49(6): 3830–3841. https://doi.org/10.1002/wrcr.20275.

Ratnam J V., Behera SK, Masumoto Y, Yamagata T. 2014. Remote effects of El Niño and Modoki events on the austral summer precipitation of Southern Africa. *Journal of Climate*, 27(10): 3802–3815. https://doi.org/10.1175/JCLI-D-13-00431.1.

Reason CJC. 2007. Tropical cyclone Dera, the unusual 2000/01 tropical cyclone season in the South West Indian Ocean and associated rainfall anomalies over Southern Africa. *Meteorology and Atmospheric Physics*, 97(1–4): 181–188. https://doi.org/10.1007/s00703-006-0251-2.

Reason CJC, Hachigonta S, Phaladi RF. 2005. Interannual variability in rainy season characteristics over the Limpopo region of southern Africa. *International Journal of Climatology*, 25(14): 1835–1853. https://doi.org/10.1002/joc.1228.

Reason CJC, Keibel A. 2004. Tropical Cyclone Eline and its unusual penetration and impacts over the Southern Africa mainland. *Weather and Forecasting*, 19(5): 789–805. https://doi.org/10.1175/1520-0434(2004)019<0789:TCEAIU>2.0.CO;2.

Reason CJC, Landman W, Tennant W. 2006. Seasonal to decadal prediction of southern African climate and its links with variability of the Atlantic ocean. *Bulletin of the American Meteorological Society*, 87(7): 941–955. https://doi.org/10.1175/BAMS-87-7-941.

Rouault M, Florenchie P, Fauchereau N, Reason CJC. 2003. South East tropical Atlantic warm events and southern African rainfall. *Geophysical Research Letters*, 30(5): 1–4. https://doi.org/10.1029/2002GL014840.

Rouault M, White SA, Reason CJC, Lutjeharms JRE, Jobard I. 2002. Ocean-atmosphere interaction in the Agulhas Current region and a South African extreme weather event. *Weather*

*and Forecasting*. https://doi.org/10.1175/1520-0434(2002)017<0655:OAIITA>2.0.CO;2.

Shongwe ME, Van Oldenborgh GJ, Van Den Hurk BJJM, De Boer B, Coelho CAS, Van Aalst MK. 2009. Projected changes in mean and extreme precipitation in Africa under global warming. Part I: Southern Africa. *Journal of Climate*, 22(13): 3819–3837. https://doi.org/10.1175/2009JCLI2317.1.

Tennant WJ, Hewitson BC. 2002. Intra-seasonal rainfall characteristics and their importance to the seasonal prediction problem. *International Journal of Climatology*, 22(9): 1033–1048. https://doi.org/10.1002/joc.778.

Thoithi W, Blamey RC, Reason CJC. 2020. Dry spell frequencies , wet day counts and their trends across southern Africa during the summer rainy season. , 1–22. https://doi.org/10.1029/2020GL091041.

Todd M, Washington R. 1999. Circulation anomalies associated with tropical-temperate troughs in southern Africa and the south west Indian Ocean. *Climate Dynamics*, 15(12): 937–951. https://doi.org/10.1007/s003820050323.

Todd MC, Washington R, Palmer PI. 2004. Water vapour transport associated with tropical-temperate trough systems over southern Africa and the southwest Indian Ocean. *International Journal of Climatology*, 24(5): 555–568. https://doi.org/10.1002/joc.1023.

Trenberth KE, Dai A, Rasmussen RM, Parsons DB. 2003. The Changing Character of Precipitation. *Bulletin of the American Meteorological Society*. American Meteorological Society, 84(9): 1205–1218. https://doi.org/10.1175/BAMS-84-9-1205.

Usman MT, Reason CJC. 2004. Dry spell frequencies and their variability over southern Africa. *Climate Research*, 26(3): 199–211. https://doi.org/10.3354/cr026199.

Vigaud N, Pohl B, Crétat J. 2012. Tropical-temperate interactions over southern Africa simulated by a regional climate model. *Climate Dynamics*, 39(12): 2895–2916. https://doi.org/10.1007/s00382-012-1314-3.

Wang G, Zhang X, Zhang S. 2019. Performance of three reanalysis precipitation datasets over the qinling-daba mountains, eastern fringe of tibetan plateau, China. *Advances in Meteorology*, 2019. https://doi.org/10.1155/2019/7698171.

Washington R, Todd M. 1999. Tropical-temperate links in southern African and Southwest Indian Ocean satellite-derived daily rainfall. *International Journal of Climatology*. https://doi.org/10.1002/(SICI)1097-0088(19991130)19:14<1601::AID-JOC407>3.0.CO;2-0.

Westra S, Fowler HJ, Evans JP, Alexander L V., Berg P, Johnson F, Kendon EJ, Lenderink G, Roberts NM. 2014. Future changes to the intensity and frequency of short-duration extreme rainfall. *Reviews of Geophysics*. Blackwell Publishing Ltd, 52(3): 522–555. https://doi.org/10.1002/2014RG000464.

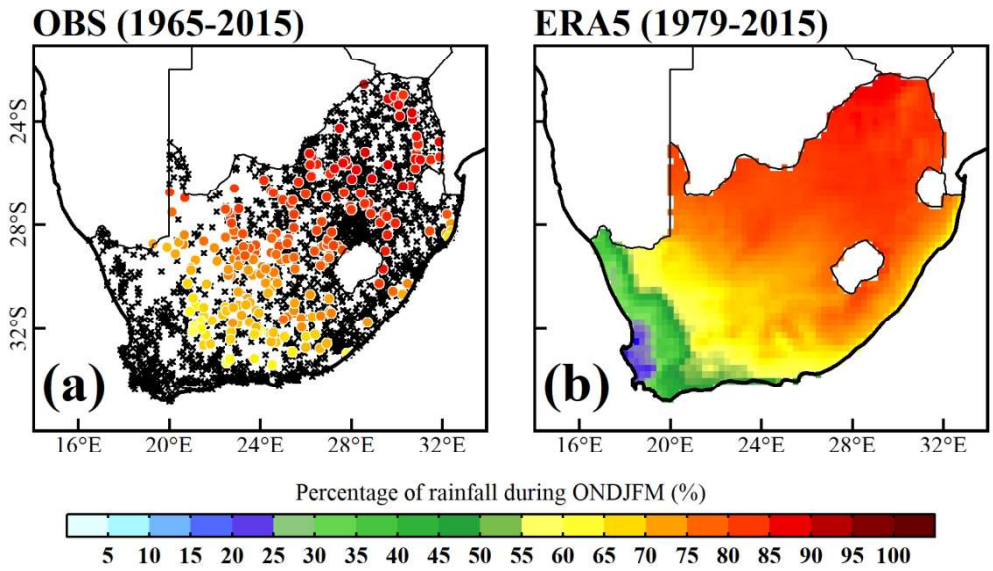


Figure 1. Spatial distribution of the percentage of rainfall during ONDJFM for OBS (a) for ERA5 (b). The unqualified stations are indicated by black "×" symbols based on the seasonality test and other quality control measures.

76x43mm (600 x 600 DPI)

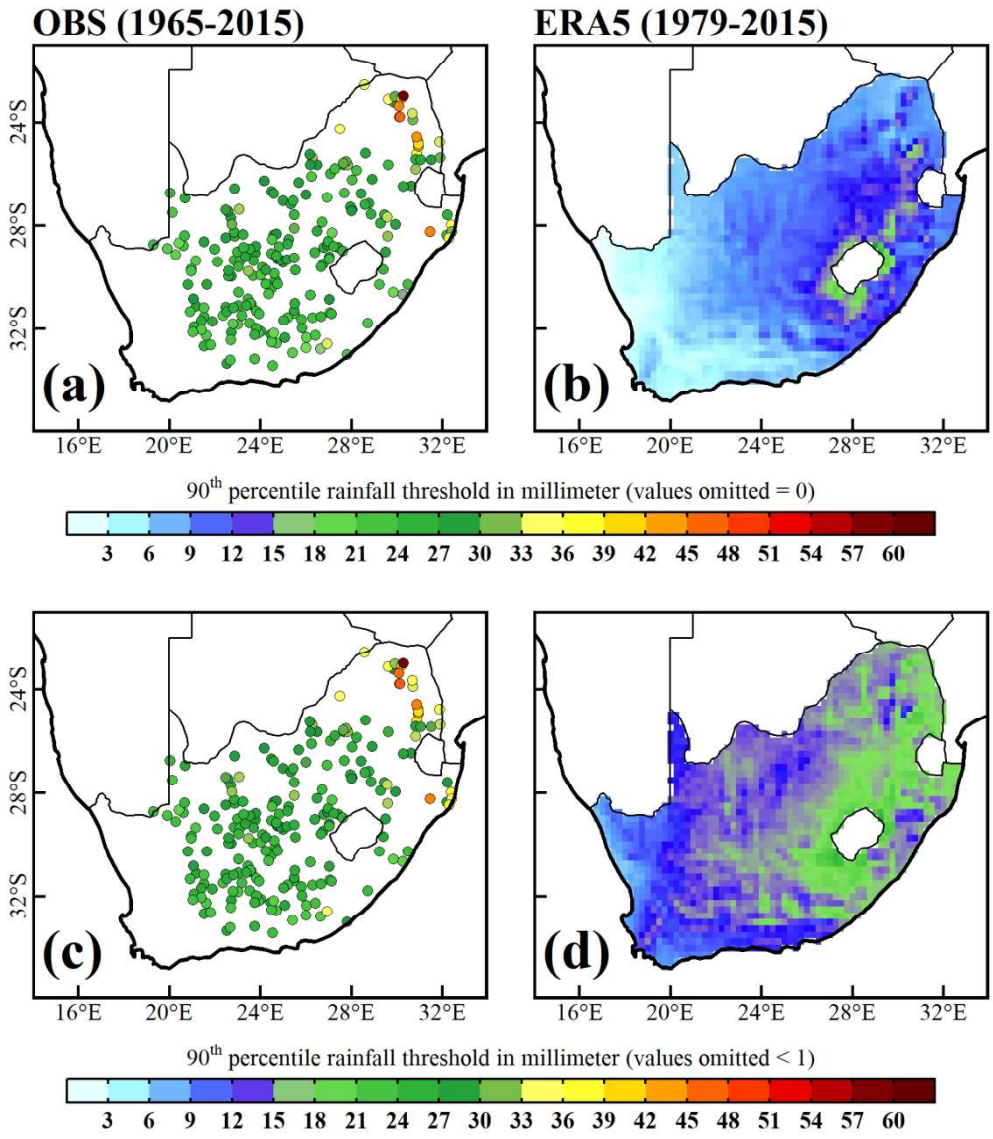


Figure 2. The 90th percentile threshold of rainfall computed after omitting the values = 0 for OBS (a) and for ERA5 (b). The 90th percentile threshold of rainfall after omitting the values <1 for OBS (c) and for ERA5 (d).

76x86mm (600 x 600 DPI)

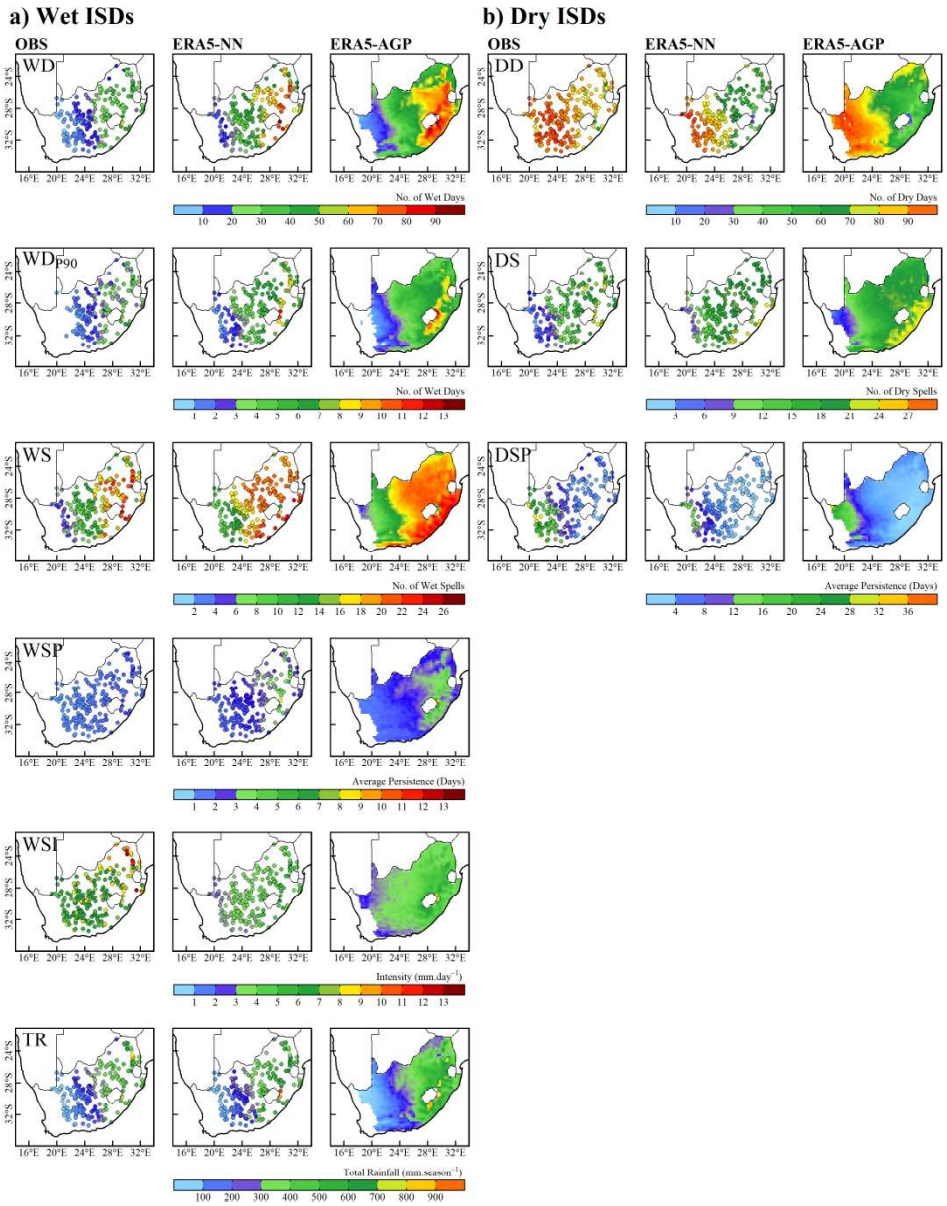


Figure 3. The average spatial distribution of ISDs, set of three column panels on the left (right) refers to the wet ISDs (dry ISDs) for OBS, ERA5−NN and ERA5−AGP. The statistics are averaged over the period of 1979−2015 for the austral summer season NDJF.

165x209mm (500 x 500 DPI)

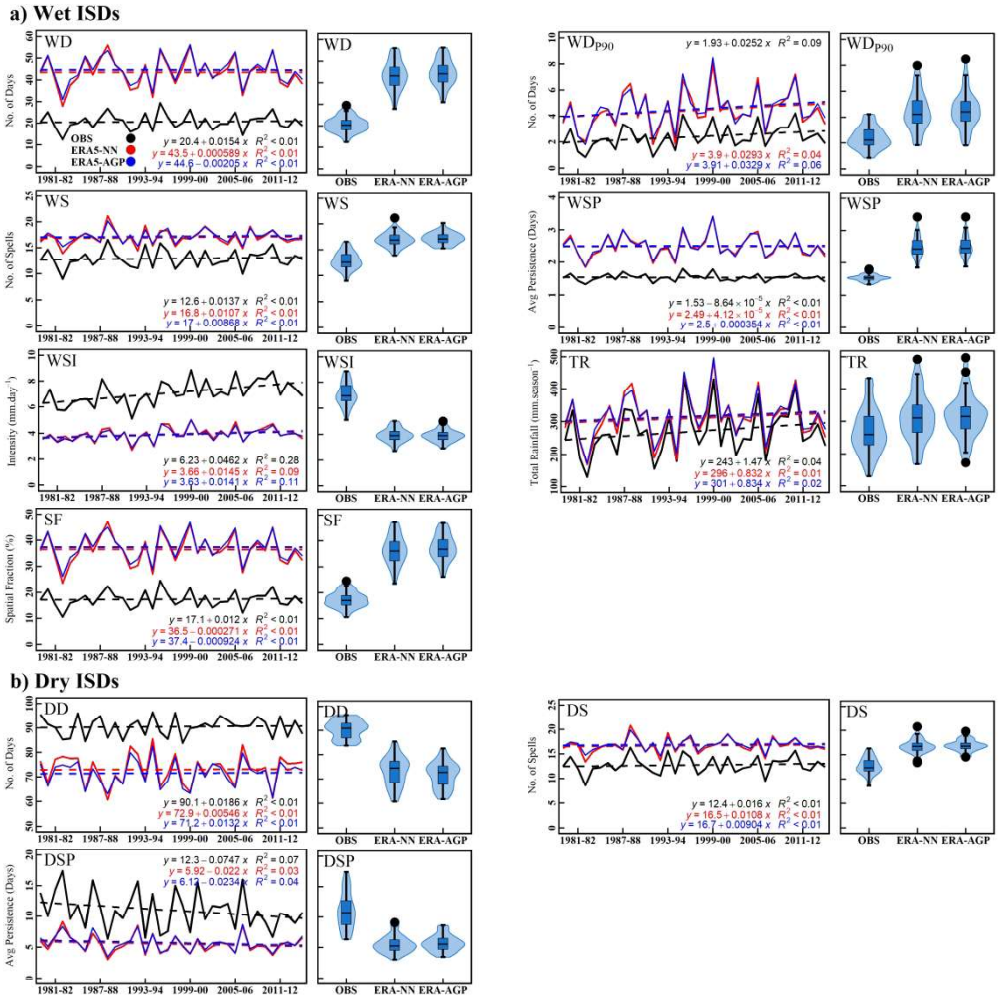


Figure 4. The average time series (line plots) and overall statistical distribution (violin plots) for wet ISDs (a) and for dry ISDs (b). The black line in each time series panel refers to the OBS, the red line is used to indicate ERA5−NN and the blue line for ERA5−AGP.

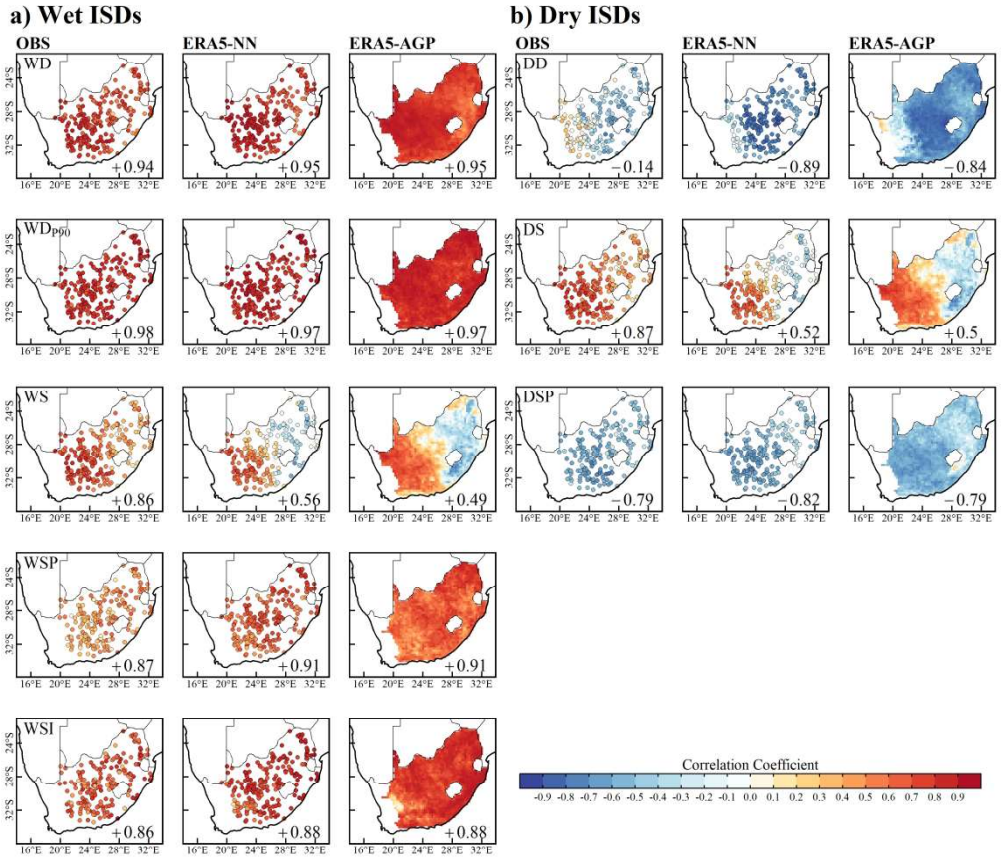


Figure 5. The spatial distribution of point-wise correlation of ISDs with total rainfall. The first set of three column panels on the left refers to the wet ISDs (a) and the set of three columns of panels on the right refers to the dry ISDs (b). The statistics are averaged over the period of 1979–2015 for NDJF using OBS, ERA5–NN and ERA5–AGP. The temporal correlations are presented in the lower right corner of each panel.

165x142mm (600 x 600 DPI)

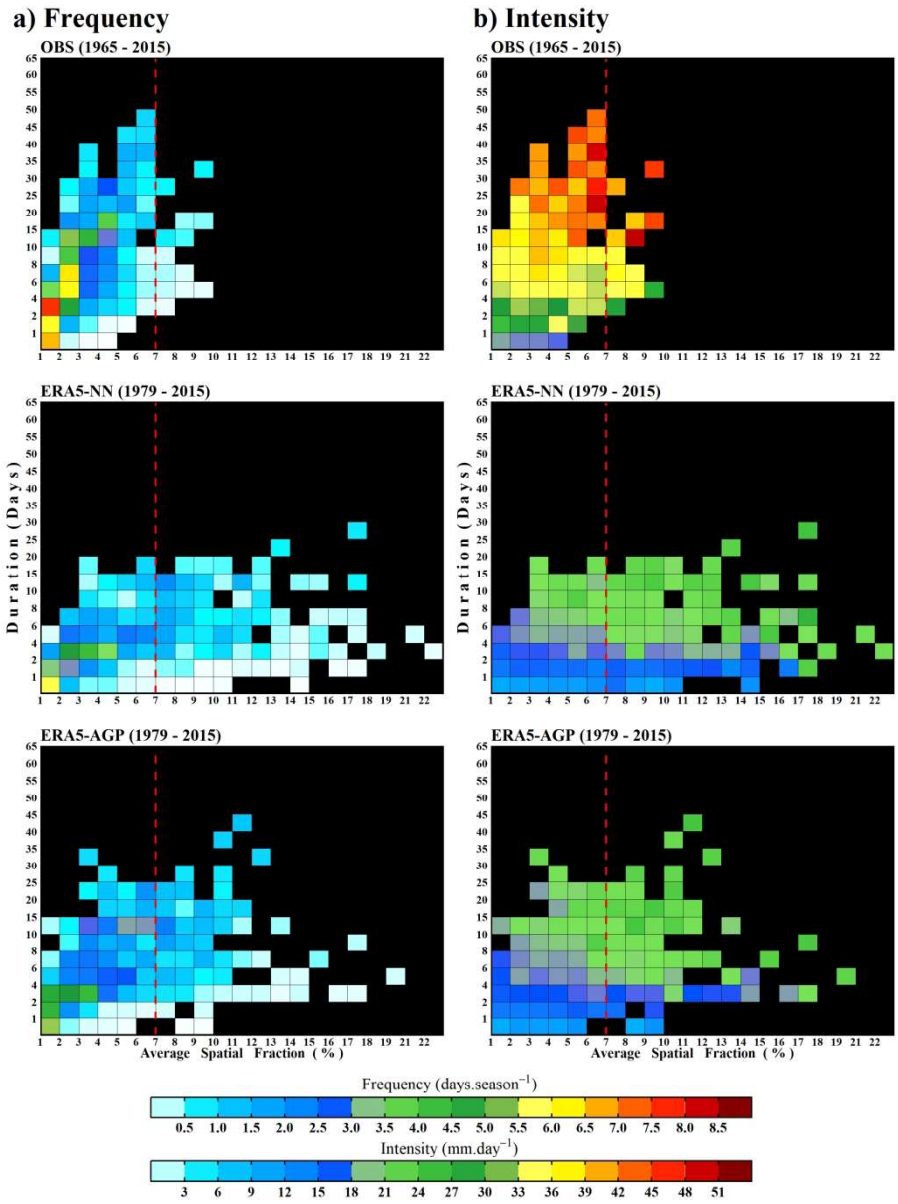


Figure 6. The frequency and intensity of extreme rainfall events as a function of average spatial fraction and duration. The set of three panels in the left column refers to frequency (a) and the set of three panels in the right column refers to intensity (b), distributed row-wise from top to bottom for OBS, ERA5−NN and ERA5−AGP respectively. The vertical red line at 7% spatial fraction separates each panel in two quadrants which distinguishes the typology of rainfall extremes. The right (left) quadrant is associated with large-scale (small-scale) extreme rainfall events.

114x152mm (600 x 600 DPI)

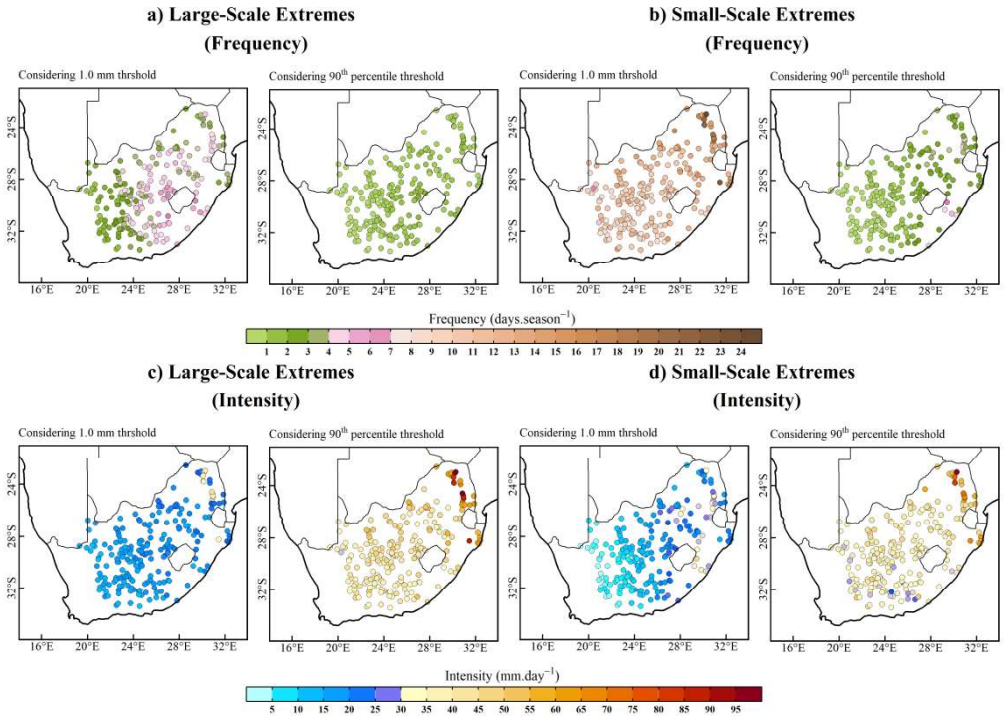


Figure 7. Average frequency computed over each station during large-scale extremes (a) and small-scale extremes (b) by considering the number of days exceeding 1.0 mm during events (left panel) and the 90th percentile during events (right panel). Same presentation for intensity in (c) and (d).

177x127mm (600 x 600 DPI)

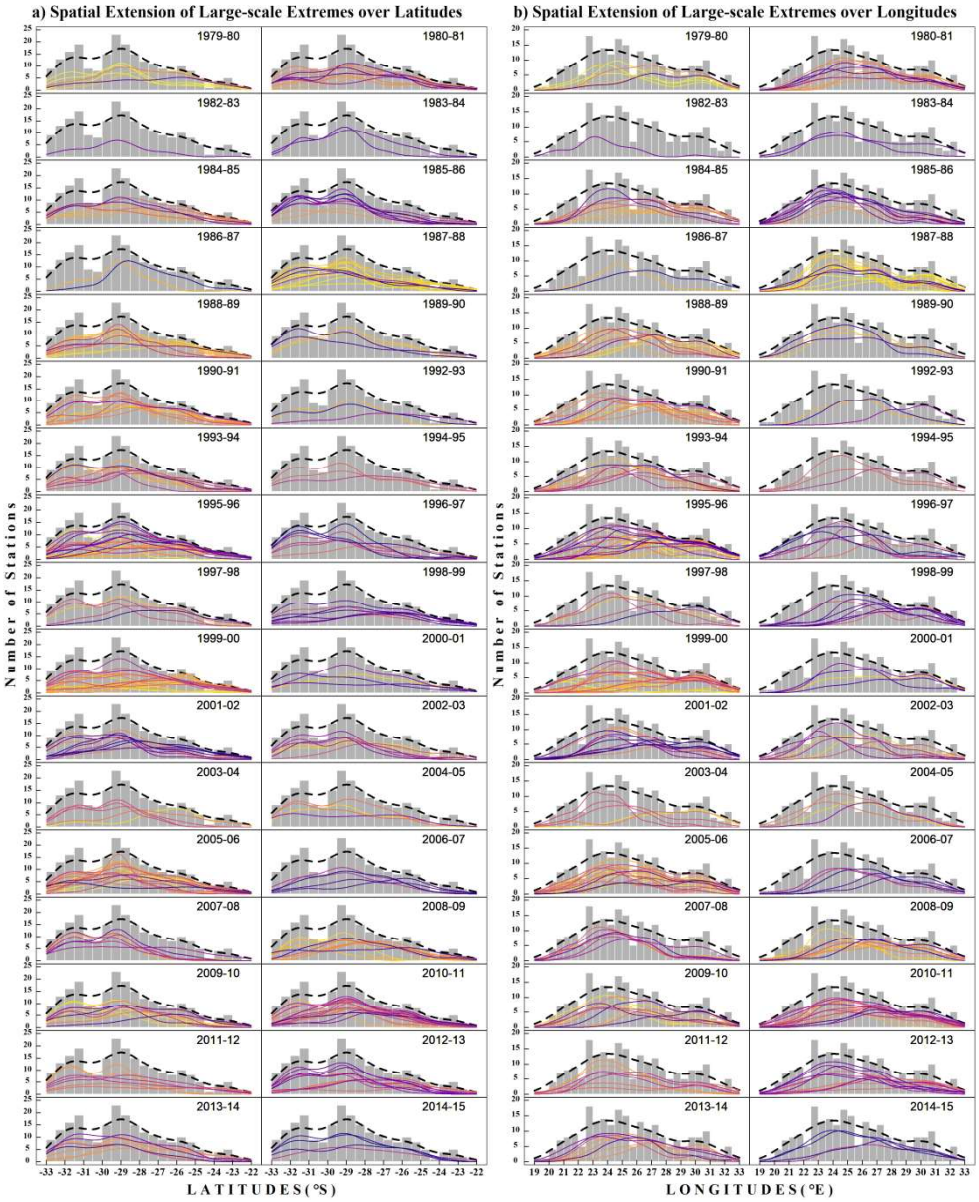


Figure 8. Spatial extension of large-scale extremes over latitudes (a) and over longitudes (b) computed by considering only those stations which exceeded 1.0 mm during large-scale extreme rainfall events with bin size = 0.5°. The histogram in each panel shows the frequency of the stations in each bin, whereas the black-dashed line in each panel represents the density of the stations provided as reference over latitudes and longitudes. Lines in distinct colors represent the density of the stations associated with each day of rainfall event in the respective seasons.

165x203mm (600 x 600 DPI)

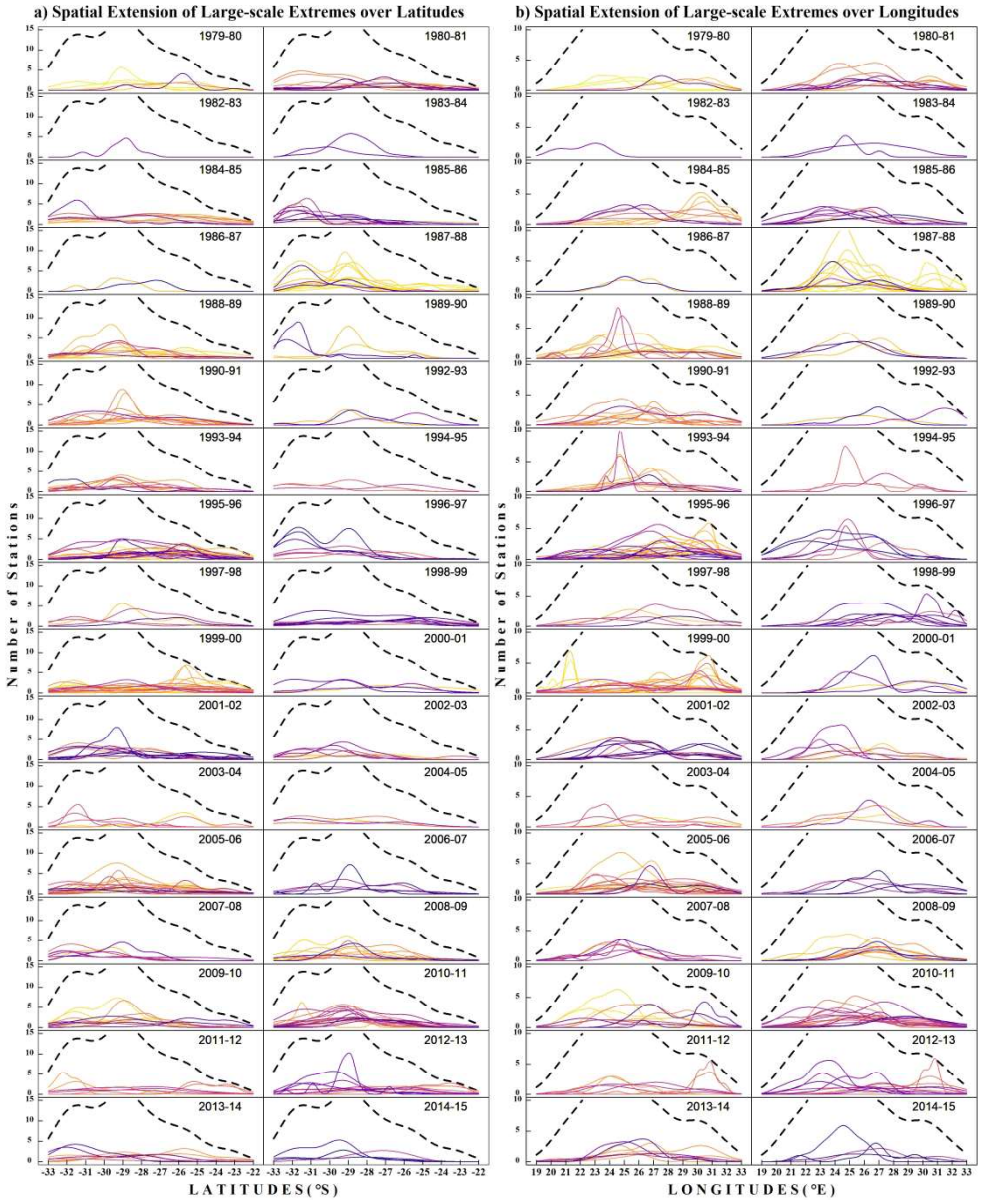


Figure 9. Spatial extension of large-scale extremes over latitudes (a) and over longitudes (b) computed by considering only those stations which exceeded the 90th percentile during large-scale extreme rainfall events with bin size = 0.5°. The black-dashed line in each panel represents the density of the stations provided as reference over latitudes and longitudes. Lines in distinct colors represent the density of the stations associated with each day of rainfall event in the respective seasons. For better visualization of density patterns, the y-axis has been reduced, and the histogram removed.

165x203mm (600 x 600 DPI)

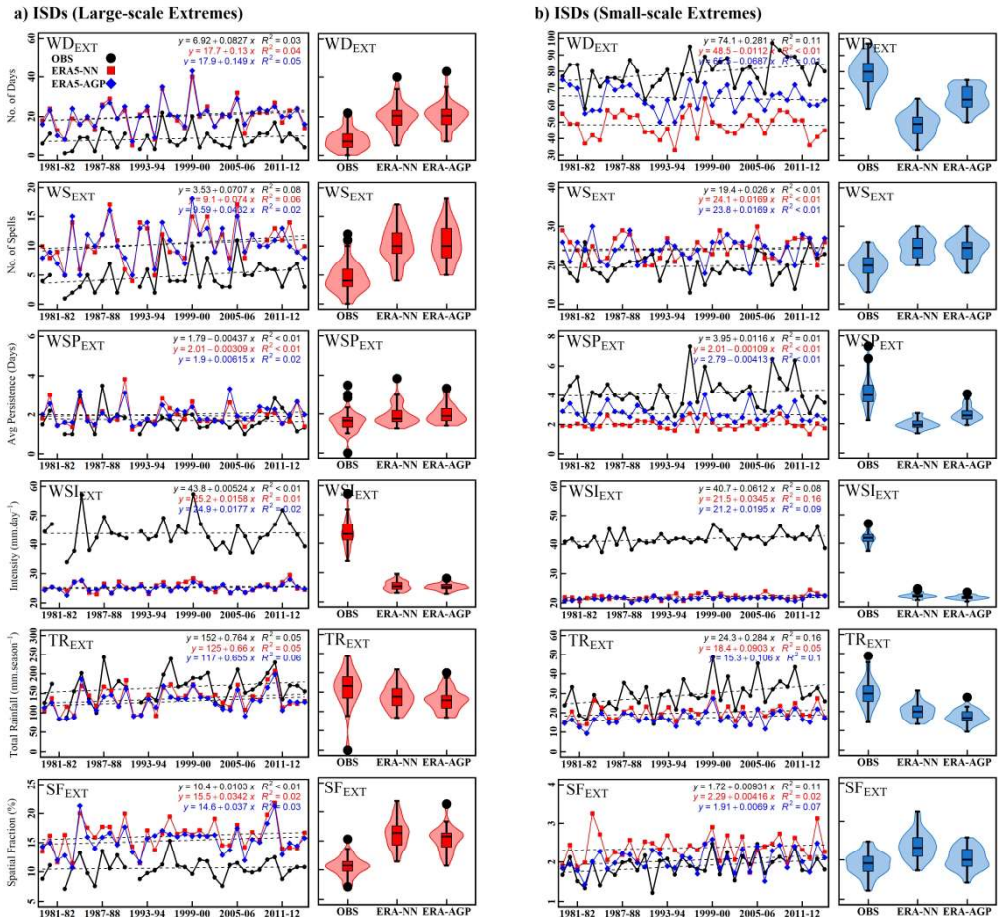


Figure 10. The average time series and overall statistical distribution (violin plots) of the ISDs associated with large-scale extremes (a) and for ISDs associated with small-scale extremes (b). The black line in each panel refers to the OBS, the red line indicates ERA5−NN and the blue line represents ERA5−AGP.

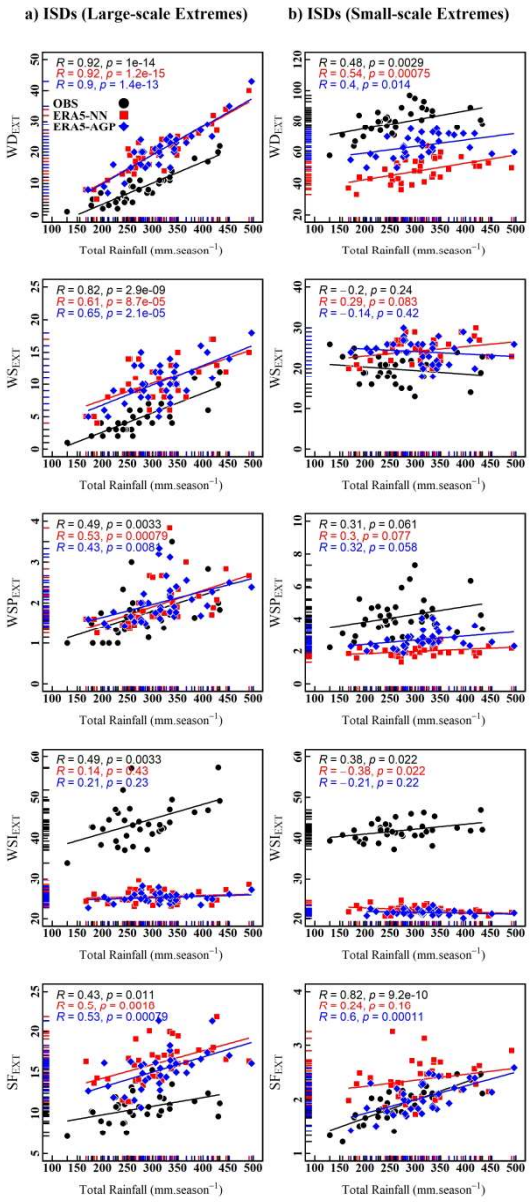


Figure 11. The scatter plot represents the statistical relationship between seasonal total rainfall and the extreme ISDs distributed row-wise from top to bottom for each descriptor. The set of five panels in the left column refers to large-scale extremes (a) and the set of five panels in the right column refers to small-scale extremes (b). In each panel OBS is indicated by the black symbol "●", ERA5−NN by the red symbols "■" and ERA5−AGP is presented in blue "◆" symbols.

88x203mm (600 x 600 DPI)

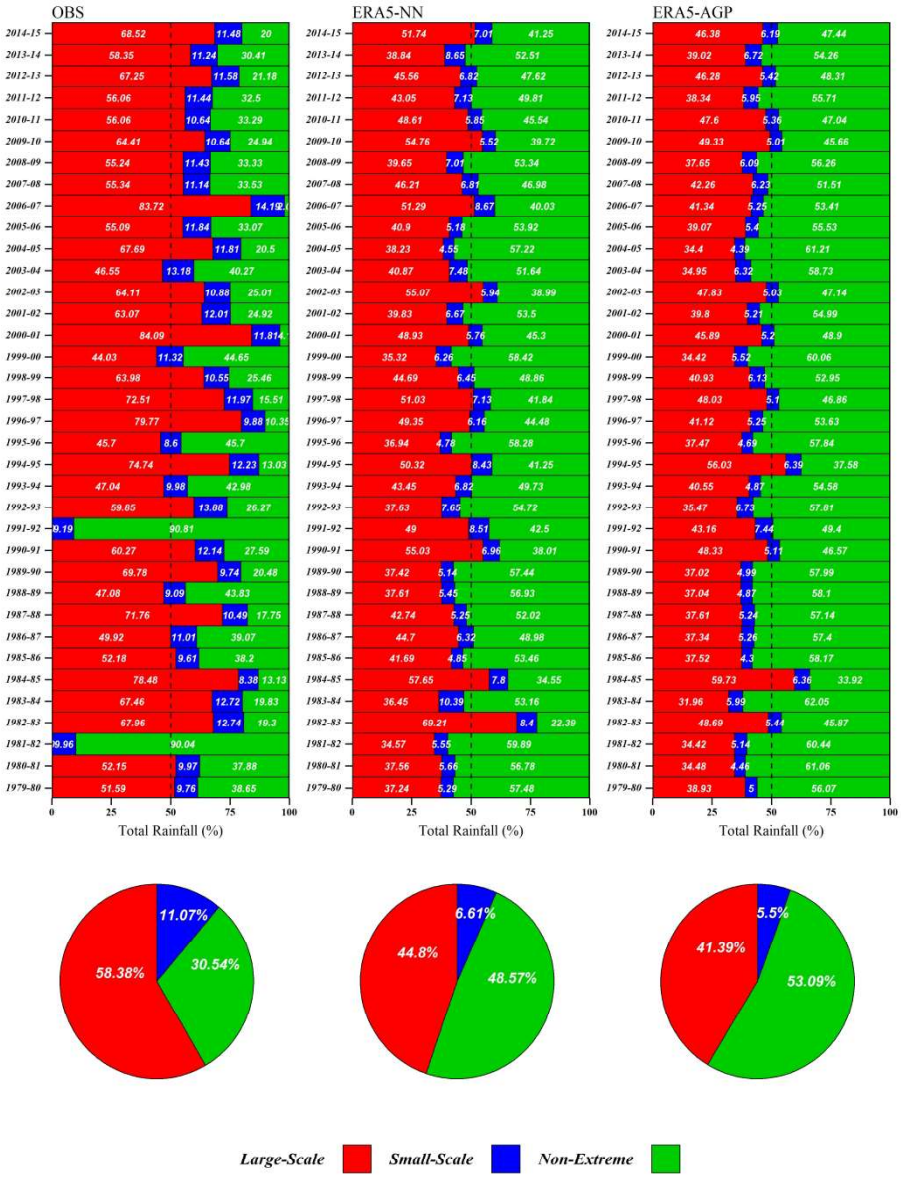


Figure 12. The stacked bar plot represents the overall contribution to the total rainfall in a season associated with large-scale extremes in red, small-scale extremes in blue and non-extreme contribution in green for OBS in the left panel, for ERA5−NN in the middle panel and ERA5−AGP in the right panel. Three pie plots at the bottom of each panel represent the overall distribution of total rainfall based on large-, small-scale and non-extreme rainfall variability averaged over the period of 1979−2015.

152x203mm (600 x 600 DPI)

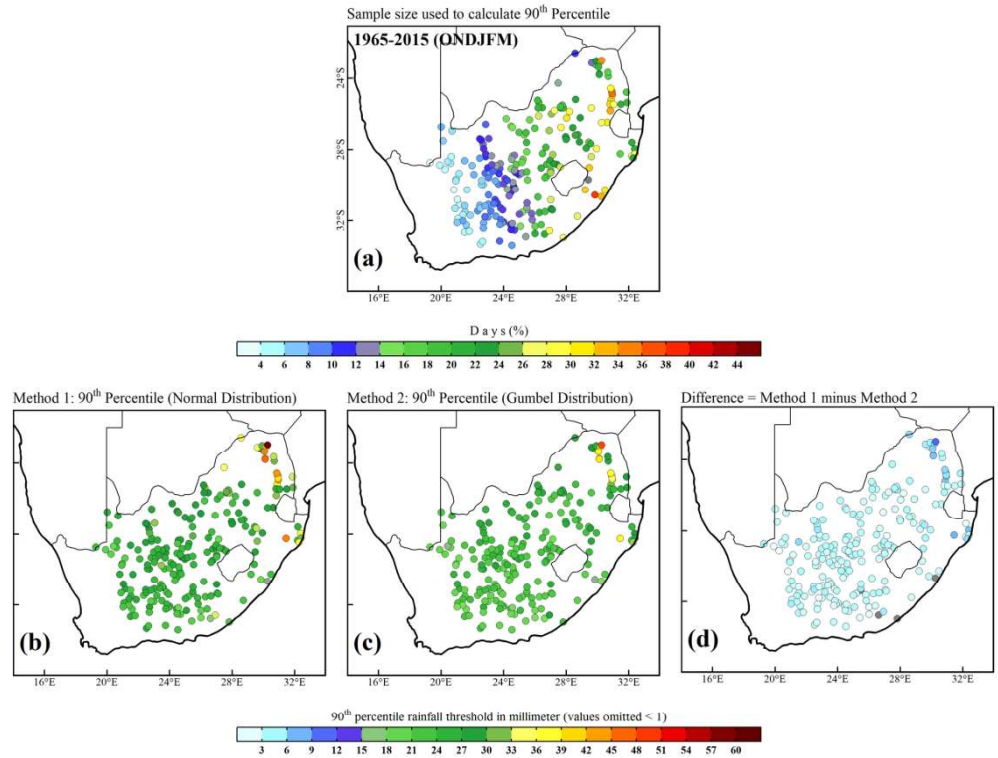


Figure. S1: Sample size used to compute 90th percentile (a), 90th percentile threshold computed by considering normal distribution (b), theoretical extreme value computed by Gumbel distribution (c) and the difference of both methods (d).

165x127mm (300 x 300 DPI)

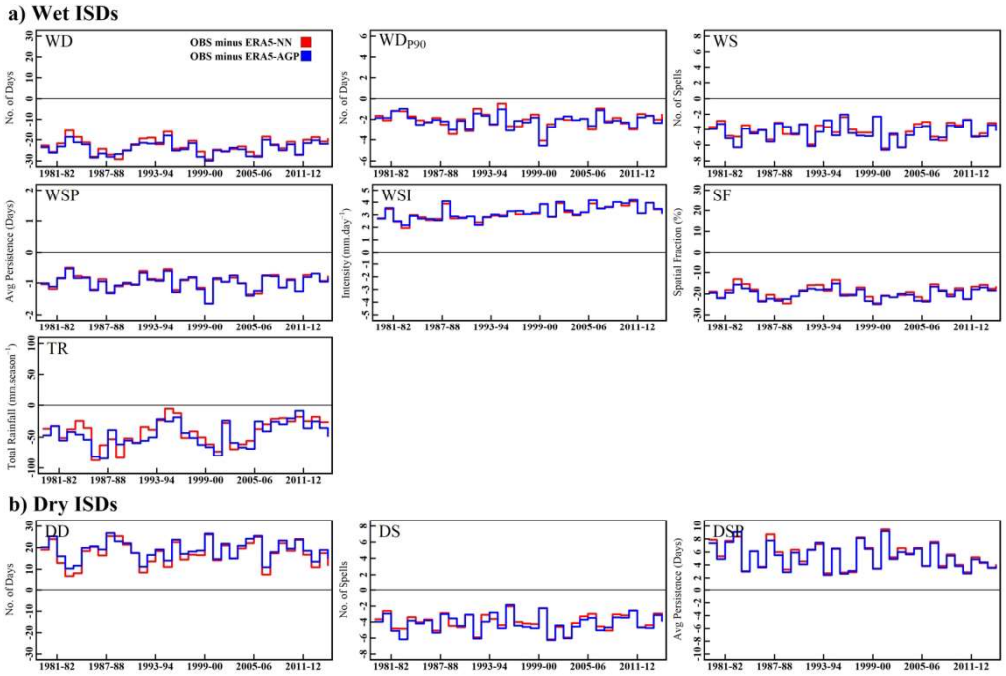


Figure. S2: The average seasonal bias of ISDs, set of first three rows containing seven panels from top refers to the wet ISDs (a) and set of three panels in bottom refers to the dry ISDs (b). OBS minus ERA5−NN is displayed by a red line and OBS minus ERA5−AGP is presented with a blue line.

165x111mm (300 x 300 DPI)

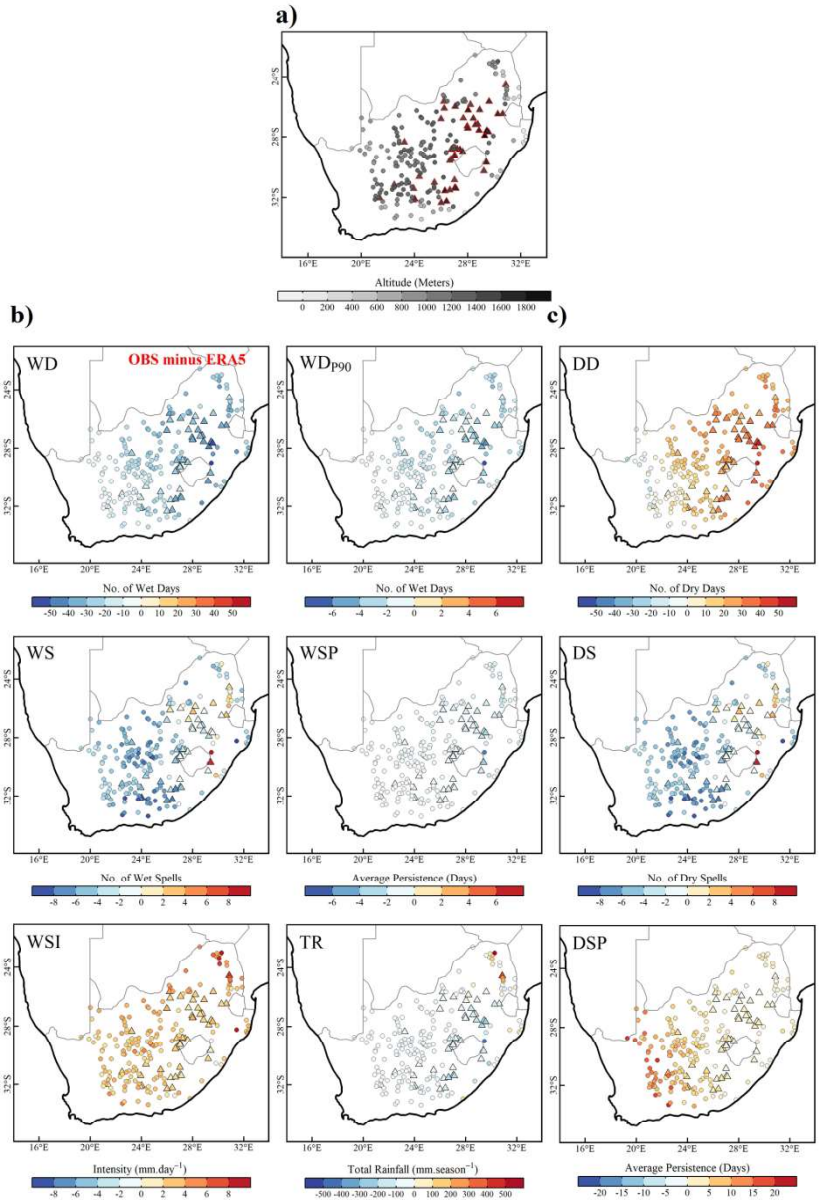


Figure. S3: Altitude of stations in meters (a). The two columns from left are associated with spatial bias in the wet ISDs (b). The third column from left is associated with spatial bias in the dry ISDs (c). The stations located at >1400 meters are indicated by triangle symbols in each panel.

152x223mm (300 x 300 DPI)

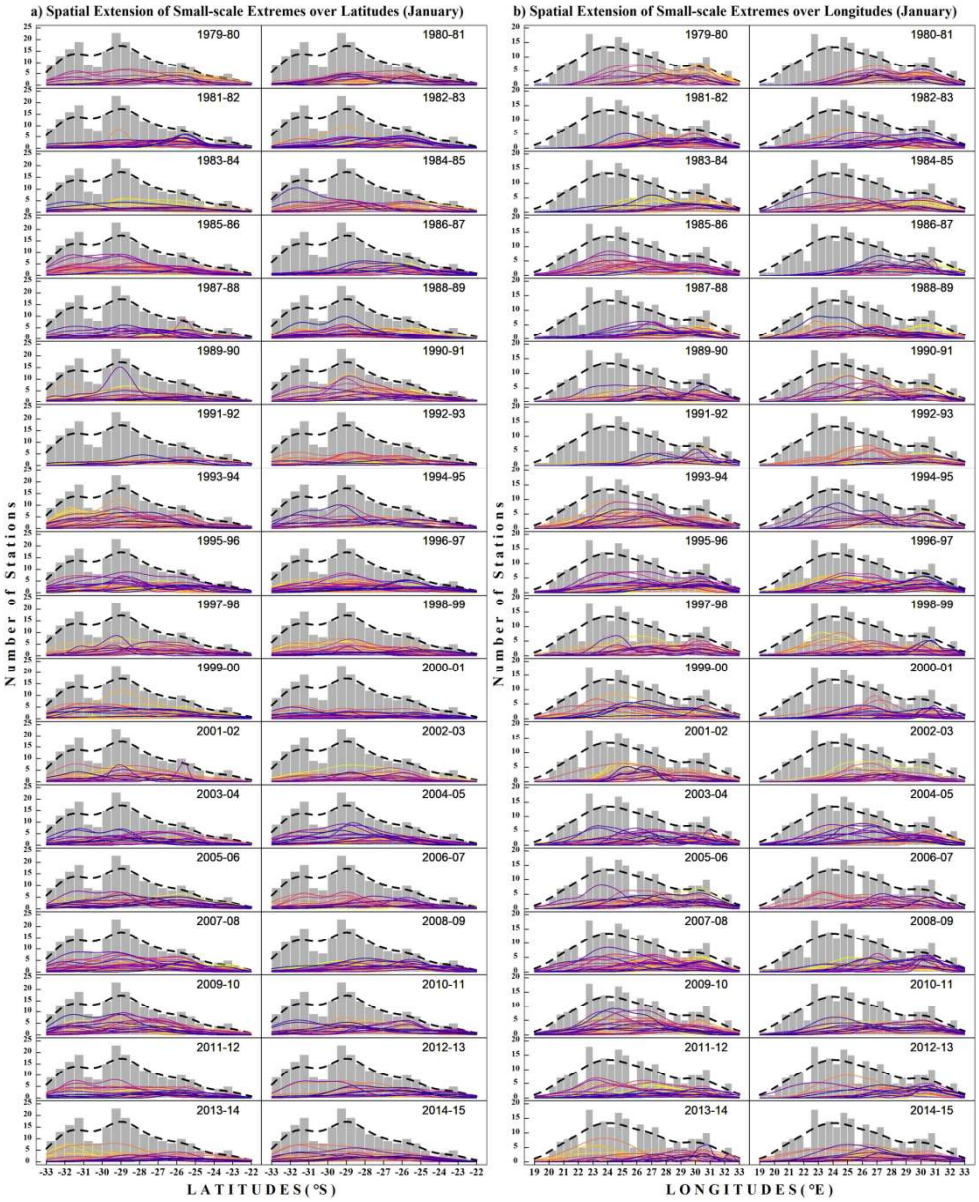


Figure S4: Same as Figure 8 but for small-scale extremes.

165x203mm (300 x 300 DPI)

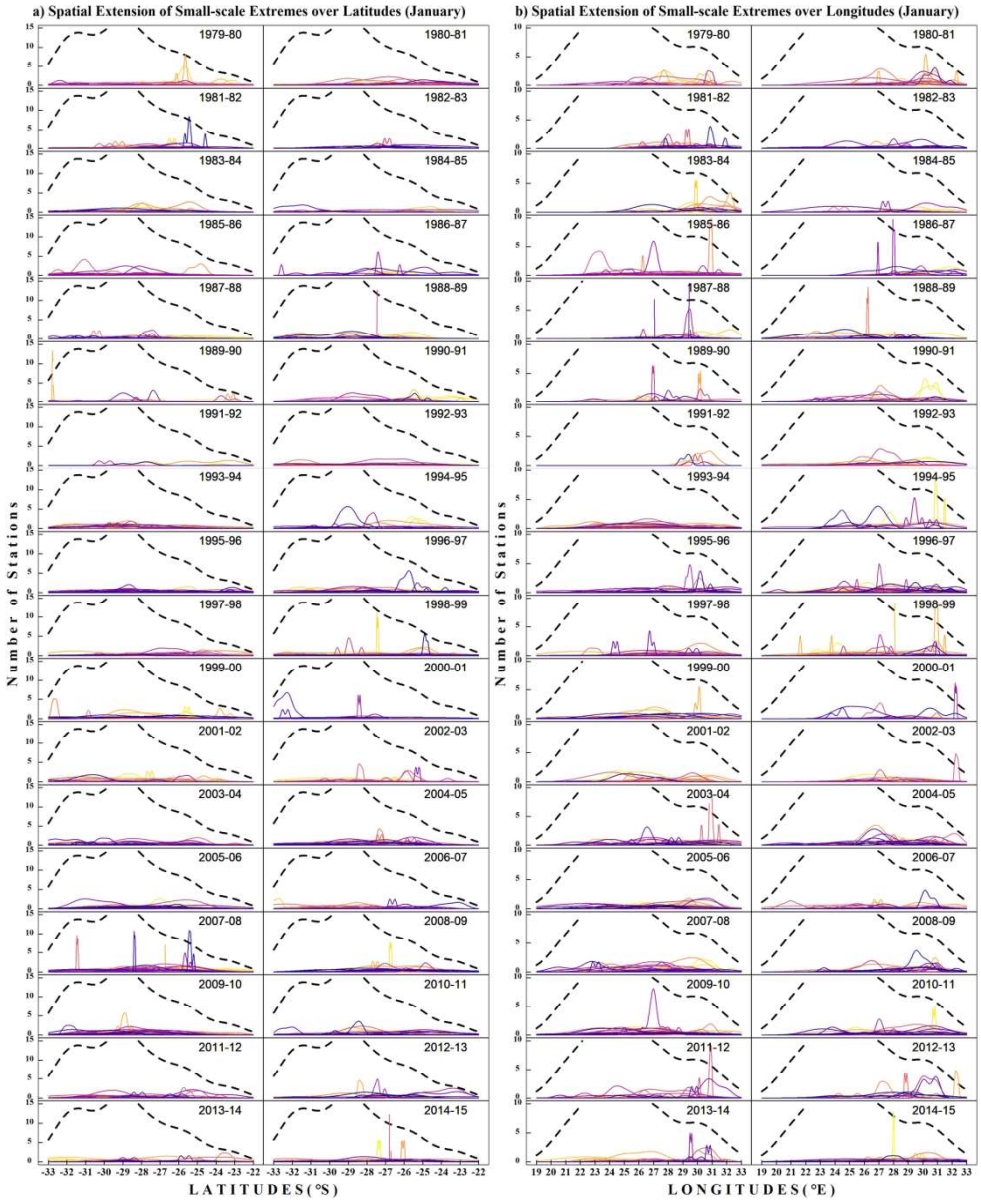


Figure S5: Same as Figure 9 but for small-scale extremes.

165x203mm (300 x 300 DPI)

**Table. 1:** The description of the wet ISDs (a) and dry ISDs (b). Columns 1−5 represent the ISD name, acronym, description, unit and scale respectively.

| **a) Wet ISDs** | | | | |
|---|---|---|---|---|
| **ISD Name** | **Acronym** | **Description** | **Unit** | **Scale** |
| Wet Days | WD | Average number of wet days in a season | Days | Seasonal |
| Wet Days >90th Percentile | $WD_{P90}$ | Average number of days exceeding the 90th percentile threshold | Days | Seasonal |
| Wet Spells | WS | Average number of wet spells in a season | Spells | Seasonal |
| Wet Spell Persistence | WSP | Average persistence of wet spells in a season | Days | Seasonal |
| Wet Spell Intensity | WSI | Average intensity of wet spells in a season | $mm.day^{-1}$ | Seasonal + Daily |
| Spatial Fraction | SF | Average spatial fraction associated with total rainfall amount in a season | Percent (%) | Seasonal + Daily |
| Total Rainfall | TR | Total rainfall amount in a season | $mm.season^{-1}$ | Seasonal + Daily |
| **b) Dry ISDs** | | | | |
| Dry Spells | DS | Average number of dry spells in a season | Spells | Seasonal |
| Dry Days | DD | Average number of dry days in a season | Days | Seasonal |
| Dry Spell Persistence | DSP | Average persistence of wet spells | Days | Seasonal |

**Table. 2:** The description of extreme ISDs. Columns 1−5 represent the ISD name, acronym, description, unit and scale respectively.

| **Extreme ISDs** | | | | |
|---|---|---|---|---|
| **ISD Name** | **Acronym** | **Description** | **Unit** | **Scale** |
| Wet Days | $WD_{EXT}$ | Average number of wet days associated with large- and small-scale extreme events in a season | Days | Seasonal |
| Wet Spells | $WS_{EXT}$ | Average number of wet spells associated with large- and small-scale extreme events in a season | Spells | Seasonal |
| Wet Spell Persistence | $WSP_{EXT}$ | Average persistence of wet spells associated with large- and small-scale extreme events in a season | Days | Seasonal |
| Wet Spell Intensity | $WSI_{EXT}$ | Average intensity of wet spells associated with large- and small-scale extreme events in a season | $mm.day^{-1}$ | Seasonal + Daily |
| Spatial Fraction | $SF_{EXT}$ | Average spatial fraction associated with total rainfall amount driven by large- and small-scale extreme events in a season | Percent (%) | Seasonal + Daily |
| Total Rainfall | $TR_{EXT}$ | Total rainfall amount associated with large- and small-scale extreme events in a season | $mm.season^{-1}$ | Seasonal + Daily |

**Table. 3:** Average Statistics of ISDs in the austral summer season computed over the period 1979−2015 using OBS, ERA5−NN and ERA5−AGP. Column 1 refers to the acronym of ISD. Columns 2−9 refer to the Mean, SD, CV, RMSE w.r.t OBS, $R^2$, correlation of ISDs w.r.t OBS, correlation of ISDs w.r.t total rainfall and trend respectively.

| ISD | Mean | ± SD | CV % | RMSE w.r.t OBS | $R^2$ | CC w.r.t OBS | CC w.r.t TR | Trend |
|---|---|---|---|---|---|---|---|---|
| | | | | **OBS** | | | | |
| **WD** | 20.66 | 3.68 | 17.83 | | 0.00 | | **0.94*** | 0.03 |
| **$WD_{P90}$** | 2.39 | 0.86 | 35.76 | | 0.09 | | **0.98*** | 1.74 |
| **WS** | 12.90 | 1.70 | 13.14 | | 0.01 | | **0.86*** | 0.29 |
| **WSP** | 1.53 | 0.11 | 7.05 | | 0.00 | | **0.87*** | 0.00 |
| **WSI** | 7.09 | 0.90 | 12.76 | | 0.28 | | **0.86*** | **3.23*** |
| **SF** | 17.30 | 3.07 | 17.75 | | 0.00 | | **0.94*** | 0.07 |
| **TR** | 270.12 | 72.17 | 26.72 | | 0.04 | | | 0.99 |
| **DD** | 90.40 | 3.79 | 4.19 | | 0.00 | | −0.14 | 0.40 |
| **DS** | 12.71 | 1.73 | 13.61 | | 0.01 | | **0.87*** | 0.53 |
| **DSP** | 10.96 | 3.01 | 27.46 | | 0.07 | | **−0.79*** | −1.40 |
| | | | | **ERA5−NN** | | | | |
| **WD** | 43.53 | 6.65 | 15.28 | 23.13 | 0.00 | **0.93*** | **0.95*** | −0.23 |
| **$WD_{P90}$** | 4.44 | 1.48 | 33.41 | 2.17 | 0.04 | **0.95*** | **0.97*** | 1.19 |
| **WS** | 17.00 | 1.45 | 8.55 | 4.22 | 0.01 | **0.80*** | **0.56*** | 0.35 |
| **WSP** | 2.49 | 0.33 | 13.40 | 0.99 | 0.00 | **0.90*** | **0.91*** | −0.26 |
| **WSI** | 3.93 | 0.51 | 13.04 | 3.20 | 0.09 | **0.88*** | **0.88*** | 1.65 |
| **SF** | 36.51 | 5.55 | 15.20 | 19.43 | 0.00 | **0.93*** | **0.95*** | −0.16 |
| **TR** | 311.01 | 73.15 | 23.52 | 45.49 | 0.01 | **0.96*** | | 0.64 |
| **DD** | 73.00 | 6.03 | 8.25 | 18.18 | 0.00 | **0.49*** | **−0.89*** | 0.07 |
| **DS** | 16.66 | 1.50 | 9.00 | 4.08 | 0.01 | **0.81*** | **0.56*** | 0.38 |
| **DSP** | 5.51 | 1.37 | 24.87 | 5.77 | 0.03 | **0.89*** | **−0.82*** | −0.86 |
| | | | | **ERA5−AGP** | | | | |
| **WD** | 44.55 | 5.98 | 13.42 | 24.07 | 0.00 | **0.92*** | **0.95*** | −0.10 |
| **$WD_{P90}$** | 4.52 | 1.42 | 31.29 | 2.23 | 0.06 | **0.94*** | **0.97*** | 1.19 |
| **WS** | 17.19 | 1.14 | 6.65 | 4.43 | 0.01 | **0.77*** | **0.49*** | 0.45 |
| **WSP** | 2.51 | 0.32 | 12.94 | 1.00 | 0.00 | **0.90*** | **0.91*** | 0.00 |
| **WSI** | 3.89 | 0.45 | 11.47 | 3.25 | 0.11 | **0.88*** | **0.88*** | **2.06*** |
| **SF** | 37.36 | 4.98 | 13.33 | 20.21 | 0.00 | **0.92*** | **0.95*** | −0.01 |
| **TR** | 316.05 | 66.96 | 21.19 | 49.65 | 0.02 | **0.97*** | | 0.56 |
| **DD** | 71.49 | 5.21 | 7.29 | 19.43 | 0.00 | **0.55*** | **−0.84*** | −0.01 |
| **DS** | 16.86 | 1.19 | 7.06 | 4.29 | 0.01 | **0.79*** | **0.50*** | 0.20 |
| **DSP** | 5.69 | 1.30 | 22.85 | 5.60 | 0.04 | **0.92*** | **−0.79*** | −1.05 |

* Significant at p=0.05 according to Pearson's correlation and Mann Kendall non-parametric trend test.

**Table. 4:** Average **s**tatistics of extreme ISDs associated with large-scale extreme events (a) and small-scale extreme (b) in the austral summer season computed over the period 1979−2015 using OBS, ERA5−NN and ERA5−AGP. Column 1 refers to the acronym of ISDs. Columns 2−9 refer to the Mean, SD, CV, RMSE w.r.t OBS, $R^2$, correlation of ISDs w.r.t OBS, correlation of ISDs w.r.t total rainfall and trend respectively.

| **a) Large-scale Extremes** | | | | | | | | |
|---|---|---|---|---|---|---|---|---|
| **ISD** | **Mean** | **± SD** | **CV%** | **RMSE w.r.t OBS** | **$R^2$** | **CC w.r.t OBS** | **CC w.r.t TR** | **Trend** |
| | | | | | **OBS** | | | |
| **$WD_{EXT}$** | 8.03 | 5.35 | 66.66 | | 0.06 | | **0.93*** | 1.53 |
| **$WS_{EXT}$** | 4.88 | 2.55 | 52.28 | | 0.08 | | **0.82*** | **2.30*** |
| **$WSP_{EXT}$** | 1.70 | 0.57 | 33.21 | | 0.01 | | **0.49*** | 0.34 |
| **$WSI_{EXT}$** | 43.86 | 5.08 | 11.58 | | 0.00 | | **0.49*** | 0.74 |
| **$SF_{EXT}$** | 10.61 | 1.71 | 16.13 | | 0.00 | | **0.43*** | 1.02 |
| **$TR_{EXT}$** | 166.68 | 36.55 | 21.93 | | 0.05 | | | 1.69 |
| | | | | | **ERA5−NN** | | | |
| **$WD_{EXT}$** | 20.14 | 7.12 | 35.37 | 12.67 | 0.04 | **0.86*** | **0.92*** | 1.37 |
| **$WS_{EXT}$** | 10.47 | 3.20 | 30.57 | 6.50 | 0.06 | **0.56*** | **0.61*** | 1.28 |
| **$WSP_{EXT}$** | 1.95 | 0.55 | 28.31 | 0.74 | 0.00 | **0.43*** | **0.53*** | 0.00 |
| **$WSI_{EXT}$** | 25.49 | 1.60 | 6.27 | 19.19 | 0.01 | **0.38*** | 0.14 | 0.23 |
| **$SF_{EXT}$** | 16.14 | 2.45 | 15.19 | 6.70 | 0.02 | **0.51*** | **0.50*** | 0.26 |
| **$TR_{EXT}$** | 136.95 | 29.96 | 21.88 | 42.28 | 0.05 | **0.72*** | | 0.94 |
| | | | | | **ERA5−AGP** | | | |
| **$WD_{EXT}$** | 20.61 | 6.93 | 33.60 | 13.18 | 0.05 | **0.83*** | **0.90*** | 1.23 |
| **$WS_{EXT}$** | 10.39 | 3.22 | 30.97 | 6.39 | 0.02 | **0.59*** | **0.65*** | 0.66 |
| **$WSP_{EXT}$** | 2.02 | 0.49 | 24.37 | 0.76 | 0.02 | **0.43*** | **0.43*** | 1.50 |
| **$WSI_{EXT}$** | 25.21 | 1.18 | 4.69 | 19.49 | 0.02 | **0.36*** | 0.21 | 1.10 |
| **$SF_{EXT}$** | 15.33 | 2.30 | 15.02 | 5.91 | 0.03 | **0.53*** | **0.53*** | 0.86 |
| **$TR_{EXT}$** | 129.50 | 28.01 | 21.63 | 46.65 | 0.06 | **0.72*** | | 1.10 |
| **b) Small-scale Extremes** | | | | | | | | |
| | | | | | **OBS** | | | |
| **$WD_{EXT}$** | 79.33 | 8.84 | 66.66 | | 0.11 | | **0.48*** | 1.75 |
| **$WS_{EXT}$** | 19.83 | 3.21 | 52.28 | | 0.01 | | −0.20 | 0.76 |
| **$WSP_{EXT}$** | 4.16 | 1.09 | 33.21 | | 0.01 | | 0.31 | 0.16 |
| **$WSI_{EXT}$** | 41.86 | 2.28 | 11.58 | | 0.08 | | **0.38*** | 1.81 |
| **$SF_{EXT}$** | 1.89 | 0.29 | 16.13 | | 0.11 | | **0.82*** | 1.73 |
| **$TR_{EXT}$** | 29.57 | 7.44 | 21.93 | | 0.16 | | | **2.17*** |
| | | | | | **ERA5−NN** | | | |
| **$WD_{EXT}$** | 48.25 | 7.18 | 35.37 | 31.89 | 0.00 | **0.62*** | **0.54*** | −0.12 |
| **$WS_{EXT}$** | 24.42 | 2.90 | 30.57 | 6.29 | 0.00 | 0.01 | 0.29 | 0.49 |
| **$WSP_{EXT}$** | 1.99 | 0.33 | 28.31 | 2.37 | 0.00 | **0.55*** | 0.30 | −0.20 |
| **$WSI_{EXT}$** | 22.14 | 0.91 | 6.27 | 19.87 | 0.16 | −0.02 | **−0.38*** | **2.00*** |
| **$SF_{EXT}$** | 2.37 | 0.34 | 15.19 | 0.58 | 0.02 | **0.43*** | 0.24 | 0.86 |
| **$TR_{EXT}$** | 20.02 | 4.01 | 21.88 | 10.87 | 0.05 | **0.74*** | | 1.40 |
| | | | | | **ERA5−AGP** | | | |
| **$WD_{EXT}$** | 64.28 | 6.93 | 33.60 | 16.65 | 0.01 | **0.62*** | **0.40*** | −0.59 |
| **$WS_{EXT}$** | 24.14 | 2.95 | 30.97 | 5.43 | 0.00 | **0.42*** | −0.14 | 0.67 |
| **$WSP_{EXT}$** | 2.72 | 0.54 | 24.37 | 1.70 | 0.01 | **0.59*** | 0.32 | −0.99 |
| **$WSI_{EXT}$** | 21.49 | 0.70 | 4.69 | 20.48 | 0.13 | 0.27 | −0.04 | **2.22*** |
| **$SF_{EXT}$** | 2.04 | 0.28 | 15.02 | 0.32 | 0.07 | **0.51*** | **0.60*** | 1.43 |
| **$TR_{EXT}$** | 17.22 | 3.55 | 21.63 | 13.36 | 0.10 | **0.79*** | | 1.89 |

* Significant at p=0.05 according to Pearson's correlation and Mann Kendall non-parametric trend test.